Top Curr Chem (2014) 347: 137–192
DOI: 10.1007/128_2013_522

Published online: 24 April 2014

Gas-Phase Valence-Electron Photoemission Spectroscopy Using Density Functional Theory

Leeor Kronik and Stephan Kümmel

Abstract We present a tutorial overview of the simulation of gas-phase valence-electron photoemission spectra using density functional theory (DFT), emphasizing both fundamental considerations and practical applications, and making appropriate links between the two. We explain how an elementary quantum mechanics view of photoemission couples naturally to a many-body perturbation theory view. We discuss a rigorous approach to photoemission within the framework of time-dependent DFT. Then we focus our attention on ground-state DFT. We clarify the extent to which it can be used to mimic many-body perturbation theory in principle, and then provide a detailed discussion of the accuracy one can and cannot expect in practice with various approximate DFT forms.

Keywords Density functional theory · Many-body perturbation theory · Photoemission

Contents

L. Kronik (✉)
Department of Materials and Interfaces, Weizmann Institute of Science, Rehovoth 76100, Israel
e-mail: leeor.kronik@weizmann.ac.il

S. Kümmel (✉)
Theoretical Physics IV, Universität Bayreuth, 95440 Bayreuth, Germany
e-mail: stephan.kuemmel@uni-bayreuth.de

1 Introduction

Photoemission spectroscopy (PES) is a well-established technique for the characterization of the electronic structure (and related properties) of matter; see, e.g., [1–3] for comprehensive overviews. PES is based on the celebrated photoelectric effect, in which matter can emit electrons upon absorption of light. Discovered experimentally by Hertz in 1887 [4], the photoelectric effect was explained by Einstein in 1905 [5] in terms of the emitted electron overcoming the work function (i.e., the minimum energy required for its removal) by virtue of energy imparted from an absorbed photon. Consequently, an emitted electron retains a kinetic energy, E_k, in the vacuum, that is given by

$$E_k = h\nu - W, \tag{1}$$

where $h\nu$ is the incident photon energy and W is the work function. The basic PES experiment consists of irradiation of an appropriate sample with photons energetic enough to cause electron emission (typically in either the X-ray or the ultraviolet regime), coupled with measurement of the kinetic energy of the emitted electrons via a suitable electron analyzer. A child's view of the experimental approach (befitting of theorists attempting to explain an experimental apparatus) is shown in Fig. 1a. In the simplest model (i.e., neglecting multi-electron processes and assuming clamped nuclei), subtraction of the incident photon energy from the measured electron kinetic energy distribution should then yield the distribution of electron binding energies in the sample.

This basic idea has led, over the years, to diverse applications. The majority of these fall into one of two classes, depending on the type of the emitted electrons [1–3]. In the first class, one focuses on the emission of core-electrons, typically using X-ray photons as they are energetic enough to eject electrons even from very deep levels. The position and line-shape of kinetic energy peaks associated with core-levels are very sensitive to the chemical structure around the atom from which the core-electron is ejected. Therefore, detailed chemical information can be inferred, so much so that this method, now typically known as X-ray photoelectron spectroscopy (XPS), was once known as ESCA – electron spectroscopy for chemical analysis. An illustrative example of XPS is shown in Fig. 1b, which shows the X-ray photoemission spectrum obtained from the nitrogen 1s core level of *trans*-$[Co(NH_2CH_2CH_2NH_2)_2(NO_2)_2]NO_3$, reported by Hendrickson et al. [6].

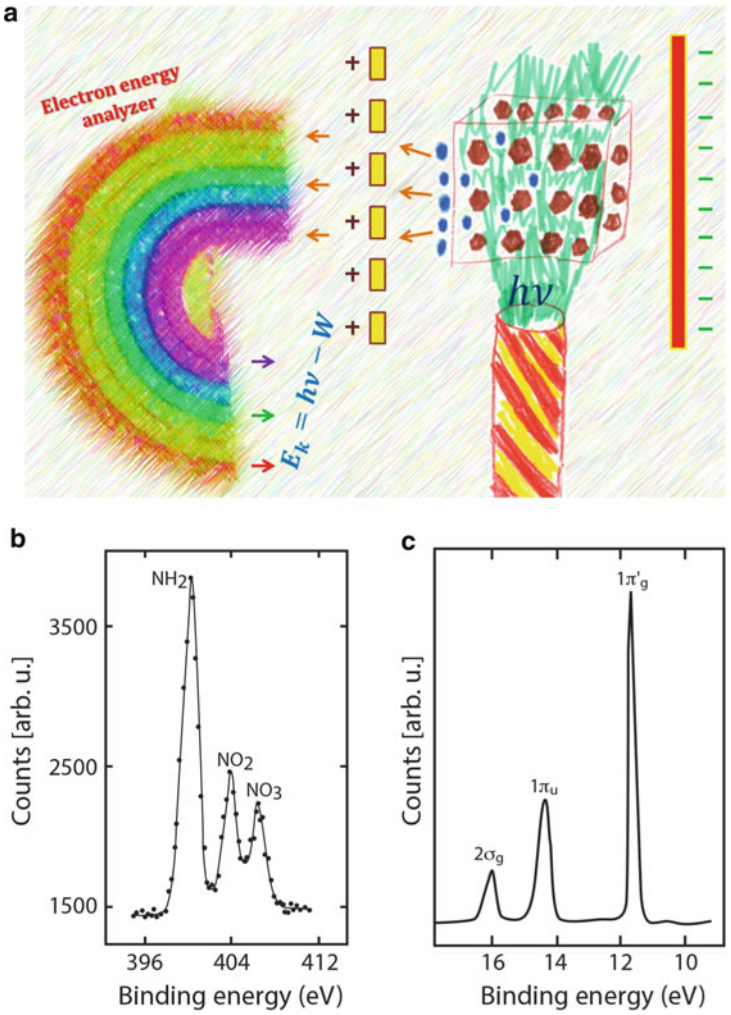

Fig. 1 Essentials of photoelectron spectroscopy. (**a**) Schematic view of the experimental approach (courtesy of Reut Baer). (**b**) X-Ray photoemission spectrum obtained from the nitrogen 1s core level of *trans*-$[Co(NH_2CH_2CH_2NH_2)_2(NO_2)_2]NO_3$ (After Hendrickson et al. [6], used with permission). (**c**) Ultraviolet photoemission spectrum obtained from Cl_2 (after Evans and Orchard [7], used with permission)

Three distinct peaks, corresponding to N in the NH_2, NO_2, and NO_3 environments, are clearly observed.

In the second class of photoemission experiments, one focuses on the emission of valence electrons, typically using ultraviolet photons for better sensitivity. With ultraviolet photoemission spectroscopy (UPS), the obtained energy distribution is then an excellent source of information on orbital hybridization and the evolution of molecular or solid-state electronic structure. An illustrative example of UPS is shown in Fig. 1c, which shows the ultraviolet photoemission spectrum of Cl_2,

reported by Evans and Orchard [7]. Three distinct peaks, attributed to the expected $2\sigma_g$, $1\pi_u$, and $1\pi_g'$ molecular orbitals, are clearly observed. Note the very different scale of binding energies in Fig. 1b, c: ~400 eV for the core levels, ~10 eV for the valence orbitals. In this chapter we focus exclusively on the latter case, i.e., on valence-electron PES.

In principle, PES can be (and has been) applied to matter in gas, liquid, or solid form. Here, we restrict our attention to the gas phase (and indeed the examples in Fig. 1 were selected accordingly). This is because, as explained in more detail below, the finite size of the system and the generally discrete nature of the electron energy levels greatly simplify the interpretation of both experiment and theory and therefore facilitate their meaningful comparison. To the best of our knowledge, the first UPS study of gas-phase valence electronic structure was reported by Turner and Al Jobory in 1962 [8]. In this pioneering study, they have provided the experimental data for several noble-gas atoms, as well as some small molecules (CS_2 and NO_2) and established the relation between the measured spectral peaks and photoionization from deeper valence electron levels. Gas-phase UPS has found many applications over the years. Here we mention two of them – cluster science and organic electronics – which we use as examples in our theoretical analysis below.

Small clusters (typically comprising up to several tens of atoms) offer a natural "bridge" between molecular and solid-state physics and chemistry. This bridge is interesting because, with increasing cluster size, all cluster properties (for example, structural, mechanical, thermal, electronic, and optical) evolve from molecular values to bulk values in non-trivial ways, often revealing new and surprising properties [9–12]. As an example, suffice it to mention that the famous C_{60} molecule was discovered in the course of studies of carbon clusters [13, 14]. Gas-phase UPS has played an important role in elucidating the electronic properties of such clusters from the very early days of modern cluster science [15–17].

In organic electronics, electronic and opto-electronic devices (e.g., transistors and light-emitting diodes) rely on conjugated organic materials with semiconducting properties, rather than on traditional inorganic semiconductors [18, 19]. The advantages offered by this emerging class of (opto-)electronic devices include cost-efficient large-area fabrication, such as direct printing methods and roll-to-roll processing, an enormous wealth of materials design through chemical synthesis, and mechanical flexibility. Many such materials are based on small organic molecules (the most common of which is pentacene). UPS of the gas-phase can then provide crucial information on the electronic structure of the basic molecular building block. Furthermore, comparison to spectroscopy of the solid-state can elucidate the degree and consequences of inter-molecular interactions – see, e.g., [20–26].

Generally, theoretical electronic structure calculations can provide crucial insights into the interpretation and ultimately the prediction of photoelectron spectra. In particular, first principles calculations, i.e., those based on the atomic species in the system and the laws of quantum mechanics, without recourse to any empirically derived information, allow insights into complex behavior which is outside the scope of simple textbook models. Of these methods, density functional

theory (DFT) [27–34] has become the method of choice for electronic-structure calculations across an unusually wide variety of disciplines, from organic chemistry [29] to condensed matter physics [35], as it allows for fully quantum-mechanical calculations at a relatively modest computational cost. However, for reasons discussed in greater detail below, the application of DFT to photoelectron spectroscopy has generated considerable controversy over the years, regarding both the limitations of the theory in principle and its performance with popular approximate forms in practice. In this chapter, we survey our recent progress in, and present understanding of, this subtle issue. We emphasize both fundamental considerations and practical applications, making appropriate links between the two.

The chapter is arranged as follows. We begin with the theory of the photoemission experiment from an elementary quantum mechanics point of view. Then we explain how this view couples naturally to the more advanced many-body perturbation theory view of photoemission. We then turn our attention to DFT. First, we discuss a rigorous approach to photoemission within the framework of time-dependent DFT (TDDFT). Then we focus on ground-state DFT. We clarify the extent to which it can be used to mimic many-body perturbation theory in principle, then provide a detailed discussion of the accuracy one can and cannot expect in practice with various approximate DFT forms. We end with concluding remarks and a brief outlook.

2 Photoemission from an Elementary Wave Function Perspective

In the following, we start from the basic principles of quantum mechanics to relate photoemission observables to the quantities that are typically accessible to electronic structure calculations. One of the basic assumptions that we make is that perturbation theory, in the sense of Fermi's golden rule, can be applied. In doing so, we exclude non-perturbative photoemission processes. For our purposes this is not a serious restriction because for elucidating the structure of the type of materials in which we are most interested – semiconductors and organic molecules – experiments are rarely done in the non-perturbative regime. We can therefore follow the usual derivation [36, 37] and start from the observation that, according to Fermi's golden rule, the probability for a transition from an initial N-electron state $|\Psi_{\mathrm{in}}^N\rangle$ to a final state $|\Psi_{\mathrm{f}}^N\rangle$ that is triggered by a photon of energy $\hbar\omega$ of an electromagnetic field with vector potential $\mathbf{A}$ is given by

$$W_{\mathrm{in}\to\mathrm{f}} \propto \left|\left\langle \Psi_{\mathrm{in}}^N \middle| \mathbf{A}\cdot\mathbf{P} \middle| \Psi_{\mathrm{f}}^N \right\rangle\right|^2 \delta(\hbar\omega + E_{\mathrm{in}} - E_{\mathrm{f}}). \tag{2}$$

Here $\mathbf{P}$ is the momentum operator, and E_{in} and E_{f} are the initial and final state energies, respectively. For clarity we assume that the N-electron molecule is initially in its ground state Ψ_0^N with energy E_0. In writing the final state one typically

introduces an approximation: when the ionization is rapid enough for the detached photoelectron not to interact with the remaining ionized system, then the final state can be well approximated by an antisymmetrized product of the wave function $\gamma_{\mathbf{k}}(\mathbf{x})$ of the liberated electron, with $\mathbf{x} = (\mathbf{r}, \boldsymbol{\sigma})$ denoting spatial and spin degree of freedom, and the wave function $\Psi_I^{N-1}(\mathbf{x}_1, \ldots, \mathbf{x}_{N-1})$, which is the Ith eigenfunction of the $N-1$-electron Hamiltonian of the ionized system. Thus, the final state wave function takes the form

$$\begin{aligned}\Psi_{I,\mathbf{k}}^N = (\mathbf{x}_1, \ldots, \mathbf{x}_N) &= \sum_{i=1}^{N} \frac{(-1)^{i+1}}{\sqrt{N}} \Psi_I^{N-1}(\mathbf{x}_1, \ldots, \mathbf{x}_{i-1}, \mathbf{x}_{i+1}, \ldots, \mathbf{x}_N)\gamma_{\mathbf{k}}(\mathbf{x}_i) \\ &= \sum_{i=1}^{N} \frac{(-1)^{i+1}}{\sqrt{N}} \Psi_I^{N-1}(\{\mathbf{x}\backslash i\})\gamma_{\mathbf{k}}(\mathbf{x}_i).\end{aligned} \tag{3}$$

The symbol $\{\mathbf{x}\backslash i\}$ denotes the set of N coordinates from which $\mathbf{x}_i$ has been excluded. The energy of this state is $E_I + E_{\mathrm{kin}}$, where the second term is the kinetic energy of the emitted electron. Thus,

$$W_{\mathrm{in}\to\mathrm{f}} \propto \left|\left\langle \Psi_0^N \middle| \mathbf{A}\cdot\mathbf{P} \middle| \Psi_{I,\mathbf{k}}^N \right\rangle\right|^2 \delta\left(\hbar\omega + E_0 - E_I - E_{\mathrm{kin}}\right). \tag{4}$$

We now write $\mathbf{A}\cdot\mathbf{P} = \sum_{j=1}^{N} \mathbf{A}\cdot\mathbf{p}_j(\mathbf{x}_j)$ and introduce a second assumption, namely that $\mathbf{A}$ is constant in space. Then we can write the matrix element in (4) as

$$\begin{aligned}&\sum_{j=1}^{N}\sum_{i=1}^{N} \frac{(-1)^{i+1}}{\sqrt{N}} \left\langle \Psi_0^N(\{\mathbf{x}\}) \middle| \mathbf{A}\cdot\mathbf{p}_j(\mathbf{x}_j) \middle| \Psi_I^{N-1}(\{\mathbf{x}\backslash i\})\gamma_{\mathbf{k}}(\mathbf{x}_i) \right\rangle \\ &= \sum_{\substack{i,j=1 \\ i\neq j}}^{N} \frac{(-1)^{i+1}}{\sqrt{N}} \int \{d^3x\backslash i\} \left[\int d^3x_i \Psi_0^{N*}(\{\mathbf{x}\})\gamma_{\mathbf{k}}(\mathbf{x}_i)\right] \mathbf{A}\cdot\mathbf{p}_j(\mathbf{x}_j)\Psi_I^{N-1}(\{\mathbf{x}\backslash i\}) \\ &\quad + \sum_{\substack{i,j=1 \\ i=j}}^{N} \frac{(-1)^{i+1}}{\sqrt{N}} \int d^3\{x\} \Psi_0^{N*}(\{\mathbf{x}\})\, \mathbf{A}\cdot\mathbf{p}_j(\mathbf{x}_j)\Psi_I^{N-1}(\{\mathbf{x}\backslash i\})\gamma_{\mathbf{k}}(\mathbf{x}_i)\end{aligned} \tag{5}$$

In the second step we split the sum into a direct term ($i = j$) and $i \neq j$. Photoemission results from the direct term as the perturbation only acts on the liberated electron in this expression. The $i \neq j$ is responsible for other effects, e.g., Auger transitions [36]. Therefore, we make a third approximation and drop this term from our considerations. The transition matrix element can then be written approximately as

$$\left\langle \Psi_0^N \middle| \mathbf{A}\cdot\mathbf{P} \middle| \Psi_{I,\mathbf{k}}^N \right\rangle = \sum_{i=1}^{N} \frac{(-1)^{i+1}}{N} \int d^3x_i \underbrace{\left[\sqrt{N} \int \left\{ d^3x \backslash i \right\} \Psi_0^{N*}(\{\mathbf{x}\}) \Psi_I^{N-1}(\{\mathbf{x}\backslash i\}) \right]}_{:=\phi^I(\mathbf{x}_i)}$$

$$\times \mathbf{A}\cdot\mathbf{p}_i(\mathbf{x}_i)\gamma_{\mathbf{k}}(\mathbf{x}_i). \tag{6}$$

The newly introduced quantity

$$\phi^I(\mathbf{x}_i) = \sqrt{N} \int \left\{ d^3x \backslash i \right\} \Psi_0^{N*}(\{\mathbf{x}\}) \Psi_I^{N-1}(\{\mathbf{x}\backslash i\}) \tag{7}$$

is called the Dyson orbital. Much of the discussion of whether and how photoemission observables can be obtained from electronic structure calculations boils down to the question of how to approximate the Dyson orbital. There are two different traditions: obtaining Dyson orbitals within the framework of many body perturbation theory on the one hand, or using molecular orbitals as useful approximations to Dyson orbitals on the other. In the following, we examine both of these traditions more closely.

3 Photoemission from a Many-Body Perturbation Theory View

The process in which a single electron is ejected from a many-electron system can be understood intuitively by considering the concept of a quasi-particle [38]. As an electron is ejected, leaving a hole behind, all other electrons in the system respond to the presence of this extra hole. The single particle picture can be retained, however, by thinking of a quasi-hole, i.e., of an effective particle that contains (is dressed by) the effects of the relaxation of the other electrons. The ionization potential is, then, the lowest quasi-hole excitation energy, with larger binding energies corresponding to higher quasi-hole excitation energies. An entirely analogous argument can be made for electron insertion energies in terms of quasi-electrons.

A theoretical framework in which the intuitive quasi-particle view of photoemission can be justified rigorously and related to the wave function perspective of the previous section is given by many-body perturbation theory (MBPT) [39–44]. While the complete physical picture and mathematical derivation of many-body perturbation theory are rather involved, and well outside the scope of this chapter, we can still provide a concise survey of the aspects most pertinent to our purposes.

The central quantity of interest in this point of view is the single-particle Green function, $G(\mathbf{x}t, \mathbf{x}'t')$, of the many-electron system. For $t > t'$, $G(\mathbf{x}t, \mathbf{x}'t')$ can be taken as the probability amplitude for finding an electron, added to the system at

coordinates $\mathbf{x}'$ and time t', at coordinates $\mathbf{x}$ at a later time t. For $t < t'$, it corresponds to the probability amplitude for finding a *missing* electron, removed from the system at coordinates $\mathbf{x}$ and time t, to be missing at coordinates $\mathbf{x}'$ at a later time t'. The two scenarios clearly correspond closely to the above concepts of the quasi-electron and quasi-hole, respectively.

Many important properties can be extracted from the Green function (see, e.g., [45]). Among these, of chief interest here are those corresponding to the energy and probability of electron insertion or removal. In the absence of external time-dependent fields, one can assume time invariance, i.e., that the Green function only depends on the relative time, $t' - t$. A frequency-dependent Green function, $G(\mathbf{x},\mathbf{x}';\boldsymbol{\omega})$, can then be defined using a Fourier transform. Importantly. this Green function can be expressed in a form known as the Lehmann representation [45]:

$$G(\mathbf{x},\mathbf{x}';\omega) = \sum\nolimits_m \frac{\phi_m(\mathbf{x})\phi_m^*(\mathbf{x}')}{\omega_m - \omega - i\delta}. \tag{8}$$

where $\hbar\omega_m$ is the difference between the energy of the mth excited state of the ionized system and the energy of the ground state of the system, $\phi_m(\mathbf{x})$ is the Dyson orbital of (7), and δ is an infinitesimal imaginary part (positive for quasi-holes and negative for quasi-electrons), which is needed to guarantee the convergence of the Fourier transform. Furthermore, the summation in the equation is assumed to be discrete owing to the discrete nature of energy levels in a finite system. Inspection of the Lehmann representation immediately reveals how quasi-particle information is "encoded" in the Green function: it can be written as a sum of terms, in each of which the pole represents quasi-electron or quasi-hole excitation energies, and the numerator is directly comprised of Dyson orbitals, already discussed above to correspond to probability amplitudes of such excitations.

Unfortunately, the Green function is generally unknown and its evaluation from its definition would require knowledge of the ground and excited states many-electron wave functions (defined in the previous section), which is precisely what we were hoping to avoid. How, then, can the Green function be computed from other considerations? By considering a non-interacting electron gas, and treating the electron interaction as a perturbation, one can evaluate the Green function formally to all orders in the perturbation. This leads to an integro-differential equation for the Green function, known as Dyson's equation. This equation can be expressed in several equivalent forms, e.g., (in atomic units) that given by Hedin [39]:

$$\left(\omega - \frac{1}{2}\nabla_{\mathbf{x}}^2 - V_{\text{ext}}(\mathbf{x}) - V_{\text{H}}(\mathrm{x})\right)G(\mathbf{x},\mathbf{x}';\omega) - \int \Sigma(\mathbf{x},\mathbf{x}'';\omega)G(\mathbf{x}'';\mathbf{x}';\omega)d\mathbf{x}'' = \delta(\mathbf{x},\mathbf{x}'). \tag{9}$$

In (9), $V_{\text{ext}}(\mathbf{x})$ is the external potential, corresponding to electron-nucleus attraction, $V_{\text{H}}(\mathbf{x})$ is the Hartree potential, i.e., the term corresponding to classical electron-electron repulsion (it is defined more explicitly below), and Σ $(\mathbf{x},\mathbf{x}';\boldsymbol{\omega})$ is known as

the self-energy – it is the precise mathematical expression of the above-mentioned "dressing" of the electron by its environment, beyond the simple electrostatic picture of the Hartree potential.

Using the Lehmann representation of (8) in (9) leads to the Schwinger form of Dyson's equation, given (in atomic units) by

$$\left(-\frac{1}{2}\nabla^2 + V_{\text{ext}}(\mathbf{x}) + V_{\text{H}}(\mathrm{x})\right)\phi_m(\mathbf{x}) + \int \Sigma(\mathbf{x},\mathbf{x}';\varepsilon_m)\phi_m(\mathbf{x}')dx' = \omega_m\phi_m(\mathbf{x}). \tag{10}$$

Equation (10) resembles the time-independent single-particle Schrödinger equation. As with the Schrödinger equation itself, its eigenvalues correspond to energies and its eigenfunctions are related to probability amplitudes (naturally, for the extraction of probabilities the eigenfunctions need to be normalized so as to conform to (7)). However, there are key differences. First, while Dyson's equation has the form of a single-particle equation, it is in fact an exact many-particle equation, with many-electron information contained in the self-energy operator. Second, Dyson's equation does not predict steady-state energies, but rather charged excitation energies. Last, but by no means least, whereas the potential in Schrödinger's equation is a multiplicative operator, the self-energy is in general non-multiplicative, frequency-dependent, and even non-Hermitian (reflecting, e.g., finite lifetime effects).

While Dyson's equation provides an interesting and rigorous framework for the quasi-particle point of view, in the absence of further information it is still insufficient as a basis for practical computation. This is because generally the self-energy, $\boldsymbol{\Sigma}(\mathbf{x},\mathbf{x}';\boldsymbol{\omega})$, is as unknown as the Green function, $G(\mathbf{x},\mathbf{x}';\boldsymbol{\omega})$. Hedin [39] has suggested that a practical way forward can be obtained by considering an expansion of the self-energy operator in terms of the dynamically screened Coulomb interaction, $W(\mathbf{x},\mathbf{x}';\boldsymbol{\omega})$, which is related to the bare Coulomb repulsion via the inverse dielectric matrix, ε^{-1} $(\mathbf{x}, \mathbf{x}';\boldsymbol{\omega})$. This leads to a set of five coupled integral equations, from which both $\boldsymbol{\Sigma}(\mathbf{x},\mathbf{x}';\boldsymbol{\omega})$ and $G(\mathbf{x},\mathbf{x}';\boldsymbol{\omega})$ can formally be extracted. Practically, the hope is that because the screened Coulomb potential, $W(\mathbf{x}, \mathbf{x}';\boldsymbol{\omega})$, is weaker than the bare one, the self-energy expansion would converge rapidly and that, ideally, only its leading term would need to be retained. This leads to a relatively simple expression of the self-energy in terms of G and W:

$$\Sigma(\mathbf{x},\mathbf{x}';\omega) = \frac{i}{2\pi}\int d\omega' \mathrm{e}^{i\delta\omega'} G(\mathbf{x},\mathbf{x}';\omega')W(\mathbf{x},\mathbf{x}';\omega-\omega'), \tag{11}$$

where δ is an infinitesimal convergence factor. Equation (11) is known as the GW approximation.

For (11) to be used in conjunction with (10) as a practical tool, one still needs to know how to calculate G and W. Typically, one first performs a ground-state DFT

calculation, explained in the next section, then computes G and W (and ergo $\boldsymbol{\Sigma}$) based on the DFT orbitals and solves Dyson's equation. This simplified procedure is sometimes known as a "one-shot" GW calculation or as a G_0W_0 calculation. Despite the seeming crudeness of the procedure, it often provides surprisingly accurate excitation energies, even in molecular systems where screening is usually not nearly as strong as in solids. As one representative and early example of the application of GW to molecules, consider that for silane (SiH_4) the ionization potential obtained as the lowest quasi-hole excitation energy from Dyson's equation in the G_0W_0 approximation is 12.7 eV [46], as compared to an experimental value of 12.6 eV. A similar degree of agreement between G_0W_0 and experiment and/or wave function-based theory has also been found for other small molecules, e.g., CO and BeO [47, 48]. We note, however, that agreement is not always this good, notably for the electron affinity – see, e.g., [49–51]. Also, the results of different GW calculations can differ considerably, as also exemplified by the case of Silane [52–55]. The pros and cons of refining the GW method via partial or full iteration to self-consistency and/or modified choices of the DFT starting point, as well as the limitations of the GW approximation itself in any form, constitute a topic of active and lively debate. This discussion is far too varied and contemporary to survey in any meaningful detail here. We do note, however, that this means that the "umbrella term" GW is insufficient to define uniquely a given computation, which may vary in DFT starting point, iterative approach (or lack thereof), and many additional details and approximations in the evaluation of both G and W.

4 Photoemission from a Rigorous Density Functional Theory View: Excited-State Theory

4.1 Concepts of Ground-State Density Functional Theory

DFT [27–34] is an approach to the many-electron problem in which the electron density, rather than the many-electron wave function, plays the central role. As already mentioned in the introduction, DFT is by far the most common first principles electronic structure theory, as it allows for fully quantum-mechanical calculations at a relatively modest computational cost. It is therefore of great interest to assess how the theory of photoemission, which we have already examined from the many-body wave function and the many-body perturbation theory points of view, can be rigorously captured within DFT.

Just as with MBPT, the complete physical picture and mathematical derivation of DFT are rather involved and are well outside the scope of this chapter. Nevertheless, here too we can still provide a concise survey of the aspects most pertinent to our purposes. The central tenet of DFT is the Hohenberg–Kohn theorem [56], which states that the *ground-state* density, $n(\mathbf{r})$, of a system of interacting electrons subject to some external potential, $v_{\text{ext}}(\mathbf{r})$, determines this potential uniquely (up to

a physically trivial constant). The importance of this theorem lies in the fact that (within the Born–Oppenheimer approximation) any system is completely described by the number of electrons in it, which is simply an integral of $n(\mathbf{r})$ over space, and by the types and positions of the nuclei in it. However, the effect of the latter two quantities on the electron system is given completely by the ion–electron attraction potential. This potential is external to the electron system and therefore, according to the Hohenberg–Kohn theorem, is uniquely determined by the ground-state density. This means that the ground-state density contains all the information needed to describe the system completely and uniquely.

The above considerations are typically not employed directly, but rather are used in the construction of the Kohn–Sham (KS) equation [57], which is the "workhorse" of DFT. In Kohn–Sham DFT, the original interacting-electron Schrödinger equation is mapped into an equivalent problem of fictitious, non-interacting electrons, such that the ground-state density of the non-interacting system is equal to that of the original system. This leads to a set of effective one-particle equations, which in spin-polarized form are given (in atomic units) by

$$\left(-\frac{\nabla^2}{2} + v_{\mathrm{ext}}(\mathbf{r}) + v_{\mathrm{H}}([n];\mathbf{r}) + v_{\mathrm{xc},\sigma}\left(\left[n_\uparrow, n_\downarrow\right];\mathbf{r}\right)\right)\varphi_{i,\sigma}(\mathbf{r}) = \varepsilon_{i,\sigma}\varphi_{i,\sigma}(\mathbf{r}), \qquad (12)$$

where $\sigma = \uparrow$ or $\downarrow$ is the electron spin z-component index, $\varepsilon_{i,\sigma}$ and $\varphi_{i,\sigma}$ are known as Kohn–Sham energies and orbitals, respectively, and $n_\sigma(\mathbf{r})$ is the electron density of spin σ, which is calculated as a sum over filled orbitals:

$$n_\sigma(\mathbf{r}) = \sum_{i=1}^{N_\sigma} \left|\varphi_{i,\sigma}(\mathbf{r})\right|^2, \qquad (13)$$

with $n(\mathbf{r}) = n_\uparrow(\mathbf{r}) + n_\downarrow(\mathbf{r})$, and N_σ the number of filled orbitals of spin σ. $v_{\mathrm{H}}([n];\mathbf{r}) = \int d^3r' n(\mathbf{r}')/|\mathbf{r} - \mathbf{r}'|$, was already mentioned as the Hartree potential. It describes the classical electron-electron Coulomb repulsion, obtained by viewing the probability distribution of the electron density as a classical distribution of electrons. $v_{\mathrm{xc},\sigma}([n_\uparrow, n_\downarrow];\mathbf{r})$ is the (spin-dependent) exchange-correlation potential, which includes all non-classical electron interactions, namely, Pauli exchange, electron correlation, and the difference between the kinetic energy of the interacting and non-interacting electron systems. The exchange-correlation potential can be expressed as a functional derivative of the exchange-correlation energy, $E_{\mathrm{xc}}([n_\uparrow,n_\downarrow])$, namely

$$v_{\mathrm{xc},\sigma}\left(\left[n_\uparrow, n_\downarrow\right];\mathbf{r}\right) \equiv \frac{\delta E_{\mathrm{xc}}}{\delta n_\sigma(\mathbf{r})}. \qquad (14)$$

Unfortunately, the exact form of E_{xc}, and consequently ν_{xc}, is not known. This is not surprising given that it has to reflect the full complexity of the original many-body problem. The practical success of DFT therefore hinges entirely on the

existence of suitable approximations for E_{xc}. The earliest, appealingly simple approximation for the exchange-correlation energy functional, already suggested by Kohn and Sham [57], is the local density approximation (LDA) or, in its spin-polarized form, the local spin density approximation (LSDA) [58, 59]. In this approximation, we assume that at each point in space the exchange-correlation energy per particle is given by its value for a homogeneous electron gas, $e_{\mathrm{xc}}(n_\uparrow(\mathbf{r}), n_\downarrow(\mathbf{r}))$, namely

$$E_{\mathrm{xc}}^{\mathrm{LSDA}}\left[n_\uparrow, n_\downarrow\right] = \int d^3r n(\mathbf{r}) e_{\mathrm{xc}}\left(n_\uparrow(\mathbf{r}), n_\downarrow(\mathbf{r})\right). \tag{15}$$

The L(S)DA has several advantages. First, $e_{\mathrm{xc}}(n_\uparrow(\mathbf{r}), n_\downarrow(\mathbf{r}))$ is unique because of the theoretical existence of a system with uniform spin densities. Second, there is ample information on e_{xc}: it was already known approximately when Hohenberg, Kohn, and Sham were formulating DFT, and has since been computed more accurately using Monte Carlo methods [60]. Furthermore, several useful analytical parametrizations of the Monte Carlo results, that also take into account other known limits and/or scaling laws of e_{xc}, have been given [61–63]. Last, but not least, the exchange-correlation potential, given by (14), becomes a simple *function*, rather than a functional, of $n_\uparrow(\mathbf{r})$ and $n_\downarrow(\mathbf{r})$. The difficulty with L(S)DA is that in real systems the density is clearly not uniform. More often than not, it actually exhibits rapid changes in space. L(S)DA was therefore expected to be of limited value in providing an accurate description of the electron interaction [57]. Nevertheless, it has often been found to provide surprisingly accurate predictions of experimental results (see, e.g., [64]), partly due to a systematic cancellation of errors between the exchange and correlation terms. More advanced approximate functionals, designed to overcome these limitations partly, are discussed in detail in Sect. 6. However, L(S)DA is sufficient to establish that DFT can indeed be a practical tool and not just a formal framework.

The degree to which single-electron DFT quantities can *approximate* quasiparticle quantities is discussed in detail in Sect. 5. However, in any case, DFT is a ground-state theory, while we are obviously trying to obtain quantities manifestly related to excitation. Rigor can therefore be restored by considering TDDFT [65–68] – a generalization of the original theory that is suitable for studies of excited states.

4.2 *Time-Dependent Density Functional Theory and Photoemission*

Just as DFT rests on the Hohenberg–Kohn theorem, TDDFT rests on the Runge–Gross theorem [69], which establishes a one-to-one correspondence between the time-dependent density and a time-dependent external potential. When the

interaction of an electronic system with light is modeled by a classical electric field that is described by a time-dependent external scalar potential, the corresponding electron dynamics can be obtained from the time-dependent Kohn–Sham equations (in atomic units):

$$\left(-\frac{\nabla^2}{2}+v_{\mathrm{ext}}(\mathbf{r},t)+v_{\mathrm{H}}([n];\mathbf{r},t)+v_{\mathrm{xc},\sigma}\left(\left[n_\uparrow,n_\downarrow\right];\mathbf{r},t\right)\right)\varphi_{i,\sigma}(\mathbf{r},t) = i\frac{\partial}{\partial t}\varphi_{i,\sigma}(\mathbf{r},t), \tag{16}$$

i.e., the time-dependent analogue of (12). The time-dependent density follows from (13) with the time-dependent orbitals replacing the static ones. In (16) the Hartree and exchange-correlation potential inherit a time-dependence from the time-dependence of the density.

In principle these equations allow for a parameter free, first principles calculation of photoemission, because the photoemission information is encoded in the time-dependent density. The latter can, in principle, be obtained exactly from (16). However, in practice the situation is more complicated, with complications arising at different levels. First, the exact time-dependent exchange-correlation potential is not known and approximations for it must be used. These approximations may need to be rather involved functionals of the density, because not only does the time-dependent $v_{\mathrm{xc},\sigma}$ share some of the intricacies of the ground-state exchange-correlation potential (such as the derivative discontinuity [70] discussed in detail in Sect. 5) but also it offers additional challenges that are not present in ground-state DFT. Prominent examples are the initial-state and memory effects [71], i.e., the dependence of the exchange-correlation functional on the initial conditions and on the history of the density and not just its present form.

Even when sufficiently accurate approximations for $v_{\mathrm{xc},\sigma}$ are known, it is not obvious how photoemission observables are to be calculated, because rigorously speaking the orbitals in (16) only serve to build the density. The physical meaning of these orbitals is discussed at length in Sect. 5, but in a traditional view that focuses only on exact relations, they are not endowed with a precise physical interpretation. Consequently, all observables should be calculated from the density. The exact, explicit density functional for the photoemission intensity is, however, so far unknown. Therefore, approximations must also be used at the level of calculating the observables. Different ways in which TDDFT allows the extraction of information about photoemission in practice, by making such approximations, are discussed in the following.

A first approach to extract photoemission information from a TDDFT calculation builds on the fact that the photoemission energies, i.e., the peaks in the recorded photoemission signal, are directly related to the eigenenergies E_I of the $N-1$ electron system that remains after detection of the photoelectron, cf. (4). If the ultimate $v_{\mathrm{xc},\sigma}$ were known, the $N-1$-electron system's ground state and

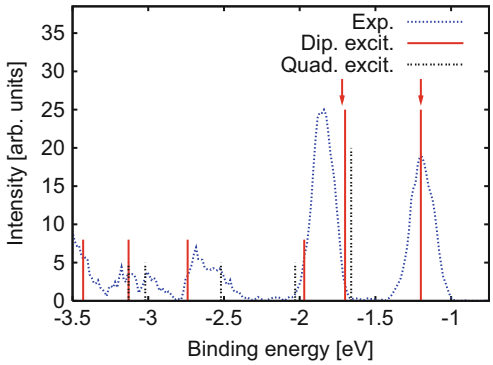

Fig. 2 Measured photoemission spectrum of a free Na_3^- cluster ("Exp.") and excitation energies calculated by TDDFT, in the adiabatic LDA approach, using real-time propagation. The energetic position of dipole ("Dip. excit.") and quadrupole ("Quad. excit.") excitations are indicated by *bars*. *Arrows* indicate the energetic position of the Kohn–Sham eigenvalues. (After [73], used with permission)

excited state energies could be calculated exactly, e.g., by transforming to the frequency domain and using TDDFT in the linear-response limit [36, 72] or by analyzing [73] the density response obtained from real-time propagation solution [74] of (16). For many systems the commonly available approximations for $v_{\mathrm{xc},\sigma}$ are accurate enough to yield excitation energies of finite systems with reasonable accuracy. Therefore, the energetic positions at which photoemission peaks can occur are accessible even in practice [36, 73, 75]. The problem that remains, though, is to know with which intensity a photoemission signal will be detected at each of the possible energies.

For small systems with only a few discrete and well-separated excitations, knowledge of the excitation energies alone may be sufficient for relating calculated excitations and measured photoemission intensities in a meaningful way. Figure 2 shows such a case. The measured gas phase photoelectron spectrum of the Na_3^- cluster [76] (SK gratefully acknowledges B. v. Issendorff for sending the raw experimental data for Na_3^-, in the context of his work on [77]), is compared to the excitation energies (indicated by bars) that were calculated [73] by real-time propagation of the Kohn–Sham equations with the LDA approximation for describing exchange and correlation. This is known as "adiabatic LDA" as it neglects the above-mentioned memory effects in the exchange-correlation functional. In addition to the TDDFT results, small arrows indicate the energetic positions of the two doubly occupied Kohn–Sham eigenvalues, the relation of which to the photoemission signal is discussed in detail in Sects. 5 and 6.1. For ease of comparison, all spectra were aligned such that they coincide at the highest peak. The black and red lines only indicate energetic positions and their drawn length is not physically significant but only serves as a guide to the eye. The first, strongest dipole allowed excitations are marked with long red lines, higher dipole excitations with smaller

red lines, and quadrupole excitations correspondingly with black dotted lines. The figure shows that there are electronic transitions corresponding to each peak in the spectrum, and that the TDDFT approach allows one to obtain information about the photoemission intensities at binding energies below -2 eV, which cannot be explained based on the eigenvalue approach discussed below (note that for spin-unpolarized calculations of Na_3^-, as here, there are only two eigenvalues corresponding to valence electrons). However, for this simple system it is already apparent that access to only the energetic positions, without being able to predict intensities (i.e., peak heights), is a limitation.

This limitation becomes very serious when the system of interest shows a wealth of excitations and the majority of them are not visible in the photoemission experiment. Knowing with which intensity an excitation contributes to the photoemission signal then is mandatory for a meaningful interpretation of the data. The situation can be seen in analogy to a photoabsorption calculation. Without knowing the oscillator strength that is associated with a transition, the photoabsorption spectrum cannot be predicted, because one needs the oscillator strength to distinguish between forbidden and allowed transitions. However, there is a decisive difference between the TDDFT calculation of photoabsorption and photoemission. Photoabsorption intensities are related to oscillator strengths, and the latter can be calculated from the frequency dependent dipole moment. The dipole moment is itself an explicit functional of the density and thus very naturally accessible in TDDFT. The intensity of the photoemission peaks, on the other hand, is related to the matrix element that appears in (4). This matrix element cannot – to the best of our knowledge – be simplified to yield an expression that explicitly depends on the density. Evaluating it would require knowledge of the wavefunction – but the latter is not known in (TD)DFT. Therefore, whereas excitation energies can rigorously be calculated from TDDFT, the photoemission intensities cannot.

In order to make further progress one has to invoke additional approximations. One possibility is to approximate the true correlated wavefunction Ψ_I^{N-1} of Sect. 2 by the Ith Slater-determinant of Kohn–Sham orbitals. It has been argued [78–81] that, among all non-interacting wave-functions, the Kohn–Sham Slater-determinant is likely to approximate the true wave-function best because it is density optimal. However, it is also well known that there are systems for which any single Slater-determinant is not a good approximation to the true wavefunction. Luckily, for organic systems the single Slater-determinant approximation can often be justified. When this is the case, (4) can be evaluated with Ψ_I^{N-1} replaced by either the Slater-determinant $\Psi_{\mathrm{KS},0}$ calculated from a self-consistent ground-state calculation for the $N-1$ electron system to obtain the first emission peak or, for further peaks, with the Ith excited-state Kohn–Sham Slater-determinant. The latter can be obtained from the linear-response TDDFT (for the $N-1$ electron system), given (in the Tamm–Dancoff approximation) in the form [72]

$$\Psi_{\mathrm{KS},I} = \sum_{i\mathrm{occ.}} \sum_{j\,\mathrm{unocc.}} k_{ij,I} c_j^\dagger c_i \Psi_{\mathrm{KS},0}. \tag{17}$$

Here, $c_j^\dagger$ and c_i are creation and annihilation operators referring to the Kohn–Sham single particle basis, $k_{ij,I}$ are the weights with which the i, j particle-hole transition contributes to the Ith excitation, and the sums run over all occupied or unoccupied orbitals, respectively. Using this equation, the Dyson orbital of (7) can also be approximately expressed as an overlap of Kohn–Sham Slater-determinants [37, 82].

The approach just described – calculating excitation energies within the rigorous framework of TDDFT, but for the transition strengths making the possibly far reaching approximation of using the Kohn–Sham Slater-determinant in place of the true wavefunction – is not the only way of extracting photoemission observables from TDDFT calculations. Instead of trying to tie in with the concepts of Sect. 2 and focusing on the $N-1$-electron system and its wavefunction, one can instead make the transition from traditional wavefunction-based quantum mechanics to TDDFT at an earlier stage and focus directly on the TDDFT simulation of the photoemission process. Thus, instead of the $N-1$-electron system, one directly simulates the N-electron system. With the help of (12) and (16) the corresponding computational procedure is straightforward. First calculate the ground-state of the N-electron system by solving the time-independent Kohn–Sham equations, then switch on the classical electric field in the form of an explicitly time-dependent, oscillating linear (dipole) potential and let the system evolve according to the time-dependent Kohn–Sham equations. If the $v_{\mathrm{xc},\sigma}$-approximation employed is accurate enough and the numerical representation allows for the density escaping towards large distances of the system's center, e.g., by using large real-space grids, then the resulting electron dynamics will faithfully reproduce the photoemission process in terms of the time-dependent density.

Focusing in this way on the N- instead of the $N-1$-electron system has advantages. For example, there is no need for assumptions about the nature of the state of the emitted electron, $\boldsymbol{\gamma}_{\mathbf{k}}$, that was introduced in Sect. 2, and nuclear dynamics can straightforwardly be included at the Ehrenfest level. Also, as the Kohn–Sham equations are directly solved numerically, the approach is not limited to the linear response regime, but can also be used for simulating non-perturbative photoemission, e.g., as triggered by highly intense lasers. This type of approach has therefore frequently been employed for calculating approximate average ionization probabilities, e.g., in [83–85]. By dividing space into a region close to the system in which electrons are considered bound and a region far away from the system in which electrons are considered unbound, the average ionization can be obtained by integrating the total (or orbital) density over the bound region.

For calculating the kinetic energy spectrum of the photoemitted electrons, a calculation based on (16) faces the problem of extracting the photoemission observables from the time-dependent density. In other words, a problem similar to the one described above for the $N-1$-electron TDDFT approach emerges. One solution to

this problem that has been suggested in the past is to use real-space grids [86, 87] and record the time-dependent orbitals $\varphi_{i,\sigma}(\mathbf{r}_O,t)$ at one or several observation point(s), $\mathbf{r}_O$, far from the system. Then Fourier-transform the orbitals with respect to t in order to find $\varphi_{i\sigma}(\mathbf{r}_O, \boldsymbol{\omega})$, and calculate the intensity of electrons emitted with a kinetic energy E_{kin} from the equation

$$I(\mathbf{r}_O, E_{\mathrm{kin}}) = \sum_{\sigma=\uparrow,\downarrow} \sum_{j=1}^{N_\sigma} \left|\varphi_{j\sigma}(\mathbf{r}_O, \omega = E_{\mathrm{kin}}/\hbar)\right|^2. \tag{18}$$

This procedure can be rationalized by thinking about the orbital at the recording point as a plane wave expansion, $\varphi_{j\sigma}(\mathbf{r}_O,t) = \Sigma_\omega \widetilde{c}_{j\sigma,\omega} \exp[i(\mathbf{k}\cdot\mathbf{r}_O - \omega t)] = \Sigma_{\boldsymbol{\omega}} c_{j\sigma,\omega} \exp(-i\omega t)$. The sum over the squares of the absolute values of the orbitals' (at point $\mathbf{r}_O$) Fourier-transforms (with respect to t) reflects the total probability amplitude $\sum_{\sigma=\uparrow,\downarrow}\sum_{j=1}^{N_\sigma} \left|c_{j\sigma,\omega}\right|^2$, with which a plane wave of energy $\hbar\omega$ is detected at the observation point.

Equation (18) avoids the association of a specific orbital with a specific emission energy. It is thus more general than the interpretation relying on orbital eigenvalues that is discussed in detail in the next section. In addition, the approach very naturally allows for extracting directional information about the photoemission process: recording the orbitals at different observation points (which can be done within one calculation) allows one to calculate angularly resolved photoemission intensities in a very natural way. However, one has to note that this approach is not an exact one – it still relies on a direct interpretation of the orbitals. More formally phrased, (18) constitutes an implicit density functional for the photoemission intensity, but an approximate one.

Beyond the formal limitation, much more serious difficulties for the practical use of (18) result from seemingly "simple" technical issues. Allowing the density to escape to regions of space that are far away from the system's center precludes the use of small, atom-centered basis sets that computationally can be handled very efficiently. Instead, real space grids are employed to allow for an unbiased and accurate representation of the density in all regions of space. Real-time, real-space propagation calculations on grids as large as those required for an accurate determination of the photoemission signal are, however, computationally very time consuming. In addition, one has to ensure that the outgoing density is not reflected at the boundaries of the numerical simulation grid. This can in principle be achieved with complex absorbing potentials [88] or mask functions [89, 90]. In practice, however, it turns out that adjusting the absorbing layer such that the photoemission signal can be recorded without substantial numerical noise, without an unphysical dependence on the chosen observation point, and without disturbances due to the boundary layer, is a tedious task. The adjustment has to be done anew for each system and set of laser parameters [90, 91]. Therefore, the technique is not easy to use for large systems with a complex electronic structure.

As an alternative to the observation point method, one can invoke the concept of the Wigner transform for calculating the momentum distribution of the

photoemitted electrons. The Wigner transform of the one-body density matrix can be interpreted as a semi-classical, approximate probability distribution for finding a particle with a certain momentum at a certain position. The concept has been used in calculations with correlated wavefunctions [92] and it has been transferred to TDDFT by using the Kohn–Sham one-body density matrix

$$\rho_{\mathrm{KS}}(\mathbf{r},\mathbf{r}',t) = \sum_{j,\,\mathrm{occ}} \varphi_j^*(\mathbf{r},t)\varphi_j(\mathbf{r}',t) \tag{19}$$

instead of the interacting one-body density matrix. In addition to the Wigner function, which is not free of ambiguities itself, this involves the further assumption that the interacting one-body density matrix far from the system's center should be well represented by (19). This is again an approximation, the accuracy of which is hard to predict. However, calculations for small molecules indicate that the concept is quite useful in practice. For details on the Wigner function approach we refer the reader to [90].

In summary, TDDFT allows the calculation of excitation energies in a way that is formally correct and exact in principle. Yet, as the density functional for the photoemission intensities is not known, approximations have to be invoked for calculating observables such as the intensities. The techniques described in this section have so far almost exclusively been used for relatively small systems. This is understandable, as TDDFT calculations are computationally much more intensive than DFT calculations. Therefore, it is highly desirable to look for less demanding ways of extracting photoemission information from electronic structure calculations, preferably requiring only ground-state quantities. To which extent and how this can be achieved is the topic of the next section.

5 Photoemission from an Approximate Density Functional Theory View: Ground-State Theory

While TDDFT can provide a rigorous theoretical approach to photoemission, in light of its above-mentioned difficulties it is still clearly tempting to utilize the conceptually and computationally simpler ground-state DFT. This would be possible if we could identify the Kohn–Sham energies and orbitals, ε_i and φ_i of (12), with the quasi-particle energies and Dyson orbitals, $\hbar\omega_i$ and ϕ_i, respectively, of (10). This identification may naively appear to be obvious, as both cases involve single-electron energies and orbitals. Furthermore, it is relatively straightforward to show that, for a non-interacting electron gas, insertion of the single-electron energies and orbitals in the Lehmann representation of (8) yields the non-interacting Green function [45]. This means that ε_i, and φ_i really are the quasi-particle energies and Dyson orbitals of the non-interacting Kohn–Sham electron gas.

However, do ε_i, and φ_i correspond to the same quantities in the original, *interacting* electron system? As explained above, the Kohn–Sham electron gas is a fictitious system of non-interacting electrons in their ground state, obtained based on a unique mapping from the physical system of electrons in their ground state. The criterion leading to the KS mapping is that both systems have the same ground state density. Therefore, any physical property of the real and fictitious system which is determined directly and solely by the electron density (e.g., the electronic dipole moment) must be the same for both systems. However, any other property (e.g., the total energy, the kinetic energy, the current density, etc.) are not necessarily identical between the two systems. This means that ε_i and φ_i need not necessarily correspond to $\hbar\omega_i$ and ϕ_i of the *original* system. Strictly speaking, ε_i, φ_i are merely auxiliary devices en route to the ground state density. In fact there is nothing in the original proof of the KS construct [57] to suggest that KS single-electron quantities carry the physical meaning of corresponding many-body perturbation theory quasi-particle quantities (or, for that matter, any meaning at all).

What relations, if any, do exist then between Kohn–Sham quantities and quasi-particle properties? It is well known that the ground state density, $n(\mathbf{r})$, of a finite, bound system of electrons (whether interacting or not), decays exponentially as $r \to \infty$, with a decay constant given (in atomic units) by $2\sqrt{2I}$, where I is the fundamental ionization energy (i.e., negative of the lowest quasi-hole energy) [93, 94]. Because the physical and Kohn–Sham systems share the same density, they must possess identical ionization potentials. Hence, the energy of highest occupied molecular orbital (HOMO) of the Kohn–Sham system, ε_{H}, already established to correspond to $-I$ of the fictitious system, automatically also corresponds to $-I$ of the real system. We therefore obtain an important relation, known as the ionization potential theorem [93–96] or as "the equivalent of Koopmans' theorem in DFT":

$$-\varepsilon_{\mathrm{H}} = I \tag{20}$$

Note that the original Koopmans' theorem [97] states a relation identical to (20) as an *approximate result*, which neglects orbital relaxation upon electron ejection, within Hartree–Fock theory, which itself neglects correlation. The DFT version of this theorem is in fact stronger – it is an exact relation, not an approximate one. Because of (20), the Kohn–Sham HOMO eigenvalue should indeed, satisfyingly, correspond to the leading photoemission peak.

Encouraged by this success, we can ask whether the same conclusion can be reached for the other occupied Kohn–Sham states. Here, unfortunately, there is no such rigorous justification. In fact, in general such an identification cannot be exact [98]. While being profoundly different physically, mathematically the Kohn–Sham equation (12) differs from the Dyson equation (10) only in that the self-energy is replaced by the exchange-correlation potential. However, whereas the former operator is non-multiplicative, frequency-dependent, and non-Hermitian, the latter operator is multiplicative, frequency-independent, and Hermitian. Sham and Schlüter derived an exact relation between the self-energy operator and the

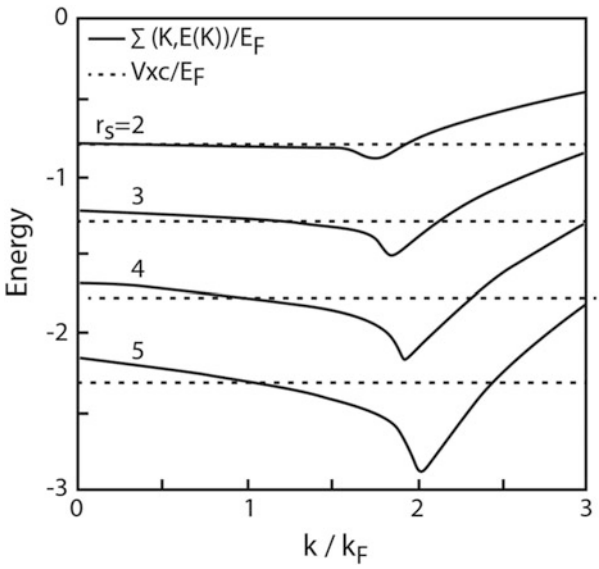

Fig. 3 The self-energy, $\Sigma(k,E(k))$, and the exchange correlation potential, v_{xc} (in units of the Fermi energy), as a function of electron crystal momentum k, for a homogeneous electron gas of several densities, expressed by the Wigner–Seitz radius, r_s, as $n = \frac{4}{3}r_s^3$. (After Jones and Gunnarson [101], used with permission)

Kohn–Sham exchange-correlation potential, by constructing an integral equation that connects these quantities and the Green function [99]. Using this relation, the Kohn–Sham exchange-correlation potential can be interpreted as the variationally best local approximation to the self-energy expression [100]. This gives us hope that the solutions of the Dyson and Kohn–Sham equations need not be completely unrelated. Nevertheless, there is no reason to think that the two equations would yield the same eigenvalues throughout.

Jones and Gunnarson [101] have explored the similarities and differences between the exact Kohn Sham eigenvalues and the quasi-particle energies by considering a case where the exact solutions are known – the homogeneous electron gas. Remember that in this case, the above-mentioned LDA is exact. The Kohn–Sham eigenvalues are then given by $\varepsilon_k = k^2/2 + v_{xc}(n)$, where k is the Kohn–Sham electron crystal momentum; The quasi-particle energies are obtained as solutions of the equation $E = k^2/2 + \Sigma(k, E)$, where $\Sigma(k, E)$ is the (known) self-energy of the homogeneous electron gas [102]. A comparative plot of $\Sigma(k,E_{QP}(k))$ and v_{xc}, for various values of the electron gas density, is given in Fig. 3. As expected, at the ionization potential (obtained for $k = k_F$, where k_F is the radius of the Fermi sphere of the homogeneous electron gas) the two quantities are identical. However, v_{xc} is a k-independent constant and therefore not generally equal to $\Sigma(k,E_{QP}(k))$. Importantly, the deviation between the two quantities away from k_F develops gradually and may even be quite small, depending on n. Furthermore, Fig. 3 shows that, for a fairly wide range around $k = k_F$, the deviation between v_{xc} and $\Sigma(k,E_{QP}(k))$ can be approximated by a straight line of small slope – a point we elaborate below.

Chong et al. [103] have provided further insight into the similarity between exact Kohn–Sham values and exact ionization energies. This was achieved by

reconstructing the exact Kohn–Sham potential from the exact density for several atomic and small molecular systems and comparing the obtained eigenvalues to experimental photoemission energies. Their results agreed very well with the above findings for the homogeneous electron gas. They found that for eigenvalues close to ε_{H} (often called outer valence orbital energies), the correspondence between Kohn–Sham theory and experiment was very close, with deviations typically on the order of 0.05–0.1 eV. This deviation is at least a factor of ten better than the typical deviation with a Hartree–Fock calculation, and often close to the experimental resolution. In agreement with the above-mentioned findings of Jones and Gunnarson, for deeper levels Chong et al. found that the Kohn–Sham eigenvalues exhibited increasingly larger deviations, ultimately reaching an order of 10 eV (which is similar to the errors made by Hartree–Fock theory). Chong et al. further established that $-\varepsilon_i$ is the leading contribution to the ith quasi-particle energy, with additional contributions determined by the overlaps between the densities of the KS orbitals, as well as by overlaps between the KS and Dyson orbital densities.

Because photoemission involves the removal of electrons, up to this point we have been comparing quasi-hole energies to occupied KS orbital energies. One can also ask a closely related question on the similarities and differences between quasi-electron energies and the energies of unoccupied Kohn–Sham orbitals. This question is directly relevant when trying to interpret *inverse* photoemission spectroscopy (IPES), where photons are emitted from a sample due to its irradiation with fixed-energy electrons and the energy distribution of the emitted photons is measured [1]. Because we are unaware of any applications of IPES in the gas phase, we do not dwell on it in this chapter. However, Fig. 3 indicates that the considerations we have made for the similarities and differences between Kohn–Sham occupied orbital energies and quasi-hole energies should also apply to unoccupied (virtual) Kohn–Sham orbital energies and quasi-electron energies. However, the homogeneous electron gas of Fig. 3 is metallic. For a non-metallic system, one should still ask whether there is a relation equivalent to (20) between the electron affinity, A, and the energy of the lowest unoccupied molecular orbital (LUMO) of the Kohn–Sham system, ε_{L}. Equivalently, one should ask whether one can equate the fundamental quasi-particle gap, $E_g = I - A$, and the KS gap, $E_g^{\mathrm{KS}} = \varepsilon_{\mathrm{L}} - \varepsilon_{\mathrm{H}}$.

Unfortunately, even with the exact KS potential, the answer is no [99, 104]. This is due to a peculiar property of the exact Kohn–Sham potential – the derivative discontinuity (DD) [95]. Briefly, for any system with a non-zero fundamental gap, the derivative of the total energy with respect to particle number must be discontinuous at the N-electron point. This is simply a reflection of the discontinuity in the chemical potential, i.e., the fact that the electron removal energy is not the same as the electron insertion energy. Consider how this is reflected in the KS description of the total energy. Because the energy contributions of the external potential and the Hartree potential are continuous with respect to the density, such discontinuity can arise, in principle, from the kinetic energy of the non-interacting electrons and/or from the exchange-correlation energy. A discontinuity in the derivative of the latter would correspond to a (spatially constant [105]) discontinuity in $v_{\mathrm{xc}}([n]; \mathbf{r})$ at an

integer particle number. We refer to this potential "jump" as the derivative discontinuity (DD) [95]. Importantly, while in some cases the DD can be small, both formal considerations [99, 104] and numerical investigation [106–109] show that it is usually sizable. We emphasize that the DD may seem unintuitive, but remember that the KS potential describes the fictitious, non-interacting electron system. Therefore, it doesn't have to obey the intuition we may have for physical potentials.

We would expect that electron removal and addition, which approach the integer number of particles from opposite directions by definition, would require KS potentials differing by the DD (an expectation borne out by more formal arguments – see, e.g., [28, 104, 110–113]. Therefore, the relations $-\varepsilon_{\mathrm{H}} = I$ and $-\varepsilon_{\mathrm{L}} = A$ cannot be satisfied simultaneously if the DD is non-zero. Choosing to uphold the former equality, as in (20), means that $-\varepsilon_{\mathrm{L}}$ will differ from A by the DD. Consequently, even with the exact functional $\varepsilon_{\mathrm{L}} - \varepsilon_{\mathrm{H}}$ is typically much smaller than $I - A$, often by many tens of percent [106–109]. In extreme cases, such as that of the Mott insulator, the KS system can even possess no gap at all, with all of the physical fundamental gap expressed in the DD [114]. Therefore, no comparison between unoccupied Kohn–Sham orbital energies and quasi-electron energies should commence until the DD is accounted for.

So far, we have discussed the relation between KS eigenvalues and quasi-particle excitation energies at length. Last, but far from least, we turn to the Kohn–Sham orbitals. Here we follow an argument given by Duffy et al. [78]. Consider again that for a non-interacting electron gas, Kohn–Sham orbitals are Dyson orbitals. Therefore, one may start with the non-interacting Kohn–Sham system and consider the difference between the self-energy Σ and the exchange-correlation potential v_{xc} as a perturbation. If one can further assume a one-to-one correspondence between Kohn–Sham and Dyson orbitals, and think of the former as a zero-order approximation for the latter, then straightforward perturbation theory yields (using spin-unpolarized notation for simplicity)

$$\phi_i(\mathbf{r}) = \varphi_i(\mathbf{r}) + \sum_{j \neq i} \varphi_j(\mathbf{r}) \frac{\langle \varphi_j | (\Sigma(\hbar\omega_i) - v_{\mathrm{xc}}) | \varphi_i \rangle}{\varepsilon_i - \varepsilon_j} \tag{21}$$

Therefore, once again the extent to which the Kohn–Sham orbitals ϕ_i and the Dyson orbitals ϕ_i resemble each other leads us right back to the extent to which the self-energy and the exchange-correlation potential resemble each other. For the same reasons already discussed above [101, 103], we can expect this resemblance to be more convincing for orbitals lying closer to the HOMO.

To summarize, it is wrong to think about the exact Kohn–Sham eigenvalues and orbitals as identical to quasi-particle energies and Dyson orbitals, except for the energy of the highest occupied state. However, it is equally wrong to think of them as completely divorced from the quasi-particle picture. In fact, they are approximations to quasi-particle quantities, the utility of which can vary, depending on the system and the sought-after degree of accuracy. To some extent, one may argue alternatively that a careful definition of the term "quasi-particle" is needed here.

Kohn–Sham particles are certainly not *Dyson's* quasi-particles. However, Kohn–Sham eigenvalues and orbitals do not describe bare electrons but interacting electrons, with the interaction effects incorporated – in the Kohn–Sham way – into the single particle properties. In this sense, the Kohn–Sham particles are a special kind of "electrons dressed with interaction effects" and one may thus say that they too are a distinct kind of quasi-particles. When thinking along these lines, one has to keep in mind, though, that they are quasi-particles of a different sort compared to what one usually refers to based on Dyson's equation, and the latter are those that are exactly related to photoemission.

6 Photoemission from Ground-State Density Functional Theory: Practical Performance of Approximate Functionals

In the previous section we explained that exact Kohn–Sham eigenvalues and orbitals can, but do not necessarily have to, serve as useful approximations to quasi-particle energies and Dyson orbitals. Using DFT to gain new insights into realistic systems, however, necessarily requires the use of approximate exchange-correlation density functionals. The practical question before us, then, is what to expect from Kohn–Sham single-electron quantities obtained using approximate exchange-correlation functionals. This question is addressed in the present section.

6.1 Semi-Local Functionals

In Sect. 4.1 we introduced the local (spin) density approximation as a useful simple approximation for the exact exchange-correlation functional. Despite its numerous successes, L(S)DA is by no means a panacea. Even when its predictions are qualitatively acceptable (which is not always the case), L(S)DA is far from perfect quantitatively. L(S)DA tends to overestimate the bonding strength, resulting in bond lengths that are too short by a few percent. It also provides an absolute error of molecular atomization energies of the order of 1 eV – much larger than the desired "chemical accuracy" of roughly 0.05 eV [115].

Many of these quantitative limitations of L(S)DA are improved significantly by using the generalized gradient approximation (GGA) for the exchange-correlation energy [115]:

$$E_{\mathrm{xc}}^{\mathrm{GGA}}\left[n_{\uparrow}(\mathbf{r}), n_{\downarrow}(\mathbf{r})\right] = \int d^3 r f\left(n_{\uparrow}(\mathbf{r}), n_{\downarrow}(\mathbf{r}), \nabla n_{\uparrow}(\mathbf{r}), \nabla n_{\downarrow}(\mathbf{r})\right). \tag{22}$$

GGA is often dubbed a "semi-local" approximation of the exchange-correlation energy. It is no longer strictly local like L(S)DA, but includes information on

deviations from homogeneity only by considering the gradients of the spin-polarized charge densities. It is called a "generalized" gradient approximation because the function $f(\cdot)$ in (22) is not obtained from a simple gradient expansion of E_{xc}. This is because, unlike L(S)DA, which is derived from a possible (though highly idealized) physical system, a simple gradient expansion is not. It therefore does not obey many formal properties of the exact E_{xc} that L(S)DA does, and the accuracy of the simple gradient expansion is often miserable.

Instead, $f(\cdot)$ in (22) is constructed so as to reproduce many important formal properties of the exact functional, e.g., the exact result in certain limits and correct scaling with respect to the density. A leading example for this approach is the popular Perdew–Burke–Ernzerhof (PBE) functional [116]. Alternatively, it can be derived by choosing a reasonable form and fitting the remaining parameters to a known data set, typically of thermochemical properties. A leading example for this approach is the Becke exchange, Lee–Yang–Parr correlation (BLYP) functional [117, 118]. In reality, the dividing line between these two types of approaches is not a sharp one because, on the one hand, empirical guidance helps in deciding which constraints are worth satisfying and, on the other hand, empirical fitting brings only very limited success if the underlying functional form is not well-motivated physically. Indeed, use of GGA functionals constructed in either way often offers a significantly improved quantitative agreement with experiment. For example, it corrects (often a bit over-corrects) for the L(S)DA overestimate of bonding strength and provides an absolute error of molecular atomization energies of the order of 0.3 eV. This is still above the desired "chemical accuracy," but much better than L(S)DA [115].

While different GGA functionals can offer a quantitative improvement over LDA, both suffer from the same formal deficiencies (discussed in more detail below) and they rarely differ qualitatively [111]. Therefore, they are discussed together here.

We have already explained that the exact Kohn–Sham exchange-correlation functional must contain a derivative discontinuity. Given their explicit density dependence, a standard LDA or GGA calculation cannot exhibit any derivative discontinuity. Instead, they approximately average it [104, 119]. Therefore, even when LDA or GGA act as good approximations for ground state properties, they underestimate the ionization potential and overestimate the electron affinity by about half the derivative discontinuity [120], such that neither is exact.

Recently, Kraisler and Kronik [121] revisited the ensemble generalization of density-functional theory to fractional electron numbers, within the framework of which the derivative discontinuity was first discovered [95]. The correct ensemble behavior requires that the total energy be piecewise-linear as a function of the fractional electron number, with a possibly discontinuous slope at the integer electron points [28, 95, 122]. Some of this discontinuity is due to the kinetic energy term and the rest is due to the DD. Kraisler and Kronik showed that explicitly requiring such a piecewise-linear dependence on electron number of the exchange-correlation energy functional, without any modification of the functional form for integer electron numbers, naturally introduces a DD into *any* approximate

exchange-correlation functional, even LDA and GGA. It does so by resulting in a non-vanishing, spatially-uniform potential that leads to a different limiting value if one approaches the integer number of electron from above or from below, which is precisely the above-mentioned desired behavior of the DD. We also note that Armiento and Kümmel have recently shown that the conventional GGA form allows one to construct an explicitly density dependent functional with a derivative discontinuity that behaves much like the exact exchange discontinuity [123]. Yet, in the following we only discuss calculations performed in the usual way, i.e., without taking ensemble-DFT potential shifts into account and without the new GGA form. However, one can still introduce, via other means, a rigid shift so as to account for the difference between the HOMO and the ionization potential. If such a rigid shift is allowed, how well do the results agree with experiment?

For simple semiconducting solids such as Si, it has long been known that all salient features of the band structure corresponding to both filled and empty states, save for the bandgap, are indeed captured rather accurately even with LDA, albeit with an effective mass that is too small (see, e.g., [124, 125]). Furthermore, for Si the LDA orbitals were found to possess a greater than 99% overlap with those obtained from full diagonalization of the self-energy in the *GW* approximation [40]. This is a first *practical* example for which we observe the general principle laid down in the previous section – Kohn–Sham eigenvalues are not exactly quasi-particle energies, but they are certainly not divorced from them, and they do provide useful information. However, bulk Si is an exceptionally convenient example, for which LDA results are very close to those obtained from the exact KS potential [106]. Therefore, while confirmation of the principles of the previous section is encouraging, is such performance to be generally expected from semi-local functionals?

For finite systems the ionization potential can be determined independently, using the same approximate density functional, simply by computing the total energy difference between the system and its cation. The eigenvalue spectrum can then be rigidly shifted, entirely from first principles, so as to set the HOMO at the total-energy-difference ionization potential value [76, 126, 127]. In some cases, this simple rigid-shift procedure is all that is needed to achieve satisfactory agreement between ground-state DFT eigenvalues and the experimental UPS data. An example is given by a UPS study of $Si_mD_n^-$ gas-phase cluster anions [126, 128]. (The original study surveyed a broad range of $4 \leq m \leq 10$ and $0 \leq n \leq 2$. For pedagogical reasons, we restrict our attention here to the subset $m = 4$, 5, 6, and $n = 0$,1.) A fundamental problem in the study of clusters is that their geometrical structure is generally unknown. Here, theory can assist by identifying low-lying isomers using simulated-annealing that is based on first principles molecular-dynamics [129, 130]. Agreement of the theoretical photoemission spectrum, obtained from the predicted structure, with the experimentally measured spectrum can then serve as evidence supporting the structure identification. We also note that in studies of clusters it is known that statistical changes to the detailed cluster geometry, due to finite-temperature effects, can be accounted for by averaging over

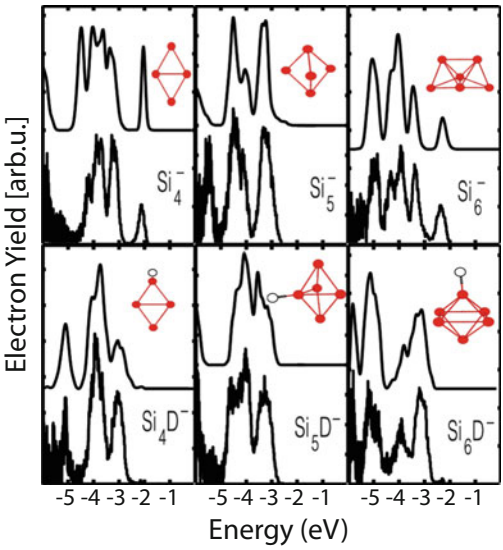

Fig. 4 Experimental UPS data (*bottom curves*), compared with theoretical LDA data, rigidly shifted from first principles such that the HOMO energy agrees with the ionization potential computed from total energy differences (see text for details of the computational approach), taken from the $Si_mD_n^-$ isomer providing the best agreement with experiment. Isomer structures are given as *insets*. After Kronik et al. [128], used with permission

a set of theoretical geometries obtained from fixed-temperature first-principles molecular dynamics [129–132]. Structural identification, followed by such averaging over eigenvalues (with all calculations, including all molecular dynamics, done only within the LDA), was performed for the above-mentioned $Si_mD_n^-$ clusters. The results are shown in Fig. 4. Clearly, for each cluster a structure can be found such that very good to excellent agreement between theory and experiment is obtained throughout. Furthermore, owing to possible kinetic effects, the structure thus identified is not necessarily the ground-state structure [126, 133]. Thus, semi-local functionals can certainly yield simulated photoemission spectra that, if rigidly shifted from first principles, allow for quantitatively useful agreement with experiment and provide useful insights into both geometrical and electronic structure.

To understand further the strengths and weaknesses of spectra obtained from semi-local functionals, we now focus our attention on the gas-phase photoemission spectrum of two small organic molecules, pentacene and 3,4,9,10-perylene-tetracarboxylic-dianhydride (PTCDA), shown schematically in Figs. 5 and 6, respectively. Both molecules are very common benchmark systems in the studies of small-molecule-based organic semiconductors and metal/organic interfaces [138]. They also happen to be highly instructive for our discussion of photoemission from DFT, and therefore will also be used to discuss the performance of other functionals in the following sections.

Rigidly shifted LDA and PBE-GGA spectra for pentacene [135, 136], compared to experiment [134] and to *GW* calculations [51, 136], are given in Fig. 5a. As with the Si cluster example above, again we see reasonable agreement between DFT and experiment. However, unlike in the previous case, agreement of the shifted spectra with experiment clearly benefits further from energy scaling of the theoretical data

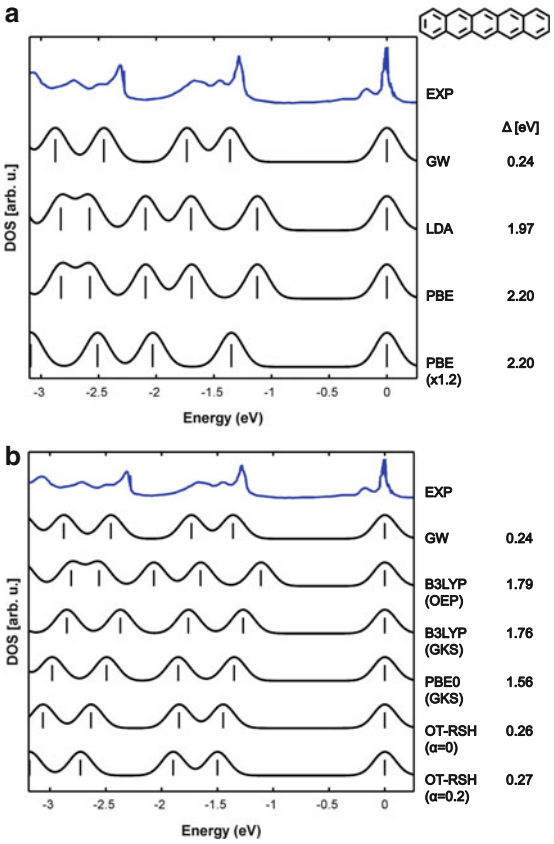

Fig. 5 Gas-phase outer-valence photoemission spectroscopy of pentacene (shown schematically in *top right corner*). (**a**) Experimental data (scanned in from Boschi et al. [134]), compared to theoretically simulated data obtained from *GW*, LDA, PBE-GGA, and energy rescaled (by 20%) PBE-GGA. (**b**) The same experimental data, compared to theoretically simulated data obtained from the hybrid functional B3LYP in both OEP and GKS form, the hybrid functional PBE0 in GKS form, and the PBE-based optimally-tuned range-separated hybrid functional with no nonlocal short-range exchange and with 20% non-local short-range exchange. All spectra in both (**a**) and (**b**) have been shifted rigidly so as to align the leading spectral peak. The size of the shift needed to align the HOMO energy with the experimental ionization potential is indicated by *Δ to the right of each theoretical spectrum*. See text for a complete description of the various theoretical methods. The theoretical data were collected from Körzdörfer and Kümmel, [135] and Refaely-Abramson et al. [136], used with permission

(i.e., "stretching" of the energy axis) [135] by a factor of ~1.2. If this factor is included (as also shown in Fig. 5a), quantitative agreement with experiment is improved. This linear stretching is clearly in accordance with the above-mentioned dominant nature of the linear corrections between self-energy and exchange-correlation potential [101] and between Kohn–Sham eigenvalues and quasi-particle energies [103, 135]. This combined "shift and stretch" procedure is often employed

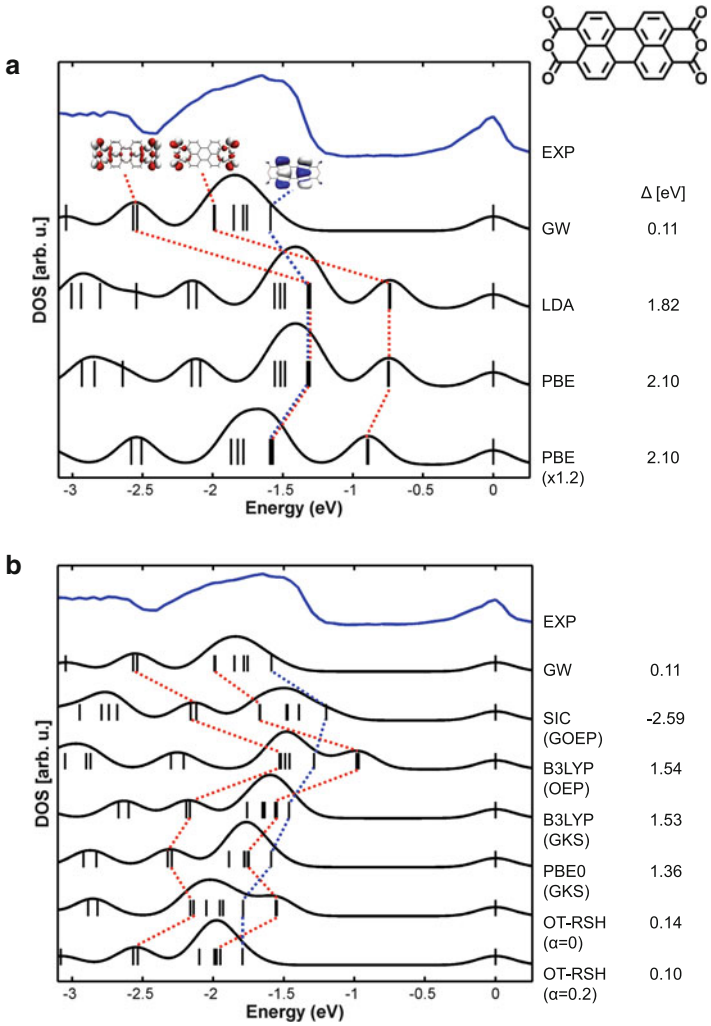

Fig. 6 Gas-phase outer-valence photoemission spectroscopy of 3,4,9,10-perylene-tetracarboxylic-dianhydride (PTCDA, shown schematically in *top right corner*). (**a**) Experimental data (from Dori et al. [23]), compared to theoretically simulated data obtained from *GW*, LDA, PBE-GGA, and energy rescaled (by 20%) PBE-GGA. (**b**) The same experimental data, compared to theoretically simulated data obtained from the a self-interaction-corrected LDA-based functional, the hybrid functional B3LYP in both OEP and GKS form, the hybrid functional PBE0 in GKS form, and the PBE-based optimally-tuned range-separated hybrid functional with no non-local short-range exchange and with 20% non-local short-range exchange. Representative orbitals of both π (*blue*) and σ (*red*) nature are also given in the figure and their corresponding eigenvalues are denoted. All spectra in both (**a**) and (**b**) have been shifted rigidly so as to align the leading spectral peak. The size of the shift needed to align the HOMO energy with the experimental ionization potential is indicated by Δ *to the right of each theoretical spectrum*. See text for a complete description of the various theoretical methods. The data were collected from Dori et al. [23], Körzdörfer et al. [137], Körzdörfer and Kümmel [135], and Refaely-Abramson et al. [136], used with permission

semi-empirically in the literature (see, e.g., [139, 140]) when interpreting photoemission data with DFT based on semi-local functionals. It is often derided as a heuristic "fudge-factor," but here we see that it has a deep and well-justified theoretical foundation. In fact it has even been recommended by Stowasser and Hoffmann as a systematic means for quantitative interpretation of Kohn–Sham eigenvalues obtained from the use of approximate exchange-correlation functionals [81].

Our next prototypical molecule, PTCDA, shows that eigenvalue spectra from semi-local functionals cannot always be remedied by a "shift and stretch" operation, as shown in Fig. 6a. By comparing LDA and PBE-GGA calculations with gas-phase experimental photoemission data and with *GW* calculation, Dori et al. [23] showed the DFT-based data to be in poor agreement with *GW* or experiment even after a rigid shift. Most glaringly, the theoretical HOMO-1/HOMO-2 peak (which is due to a doubly-degenerate eigenvalue) is found in a region devoid of any meaningful signal in either *GW* or experiment. A key observation for understanding the origin of the problem is that in PTCDA the outer-valence orbitals can be broadly classified as π-orbitals, delocalized on the perylene core, or σ-orbitals localized on the anhydride side groups. Representative orbitals of either kind are also given in Fig. 6a and their corresponding eigenvalues are denoted. Simultaneous description of localized and delocalized states is difficult with semi-local functionals, also in the solid-state (see, e.g., [141, 142]) owing to self-interaction errors [62].

What is the self-interaction error? In the Kohn–Sham equation (12) we have somewhat arbitrarily selected to partition the consequences of electron–electron interaction to a classical Coulomb part and an "everything else" exchange-correlation part. As a result, an explicit classical electron–electron repulsion potential, namely the Hartree term, arises. As mentioned above, the latter is an essentially classical expression that views the quantum charge *probability* distribution as a classical distribution of charges. This, however, means that it is inherently in error, because each electron is repelled from the total charge in the system, including a spurious repulsion from *itself*. This effect is known as the self-interaction error and was noted as early as 1934 by Fermi and Amaldi [143] in the context of Thomas–Fermi theory [144, 145] – a "forerunner" of DFT. The spurious repulsion is particularly easy to see in one-electron systems, where clearly there should be no electron–electron repulsion at all, and yet the Hartree term is not zero. Because electron–electron interaction is, in principle, handled exactly in DFT, whatever error we are making in the Hartree term must be completely canceled out by the exchange-correlation term. Unfortunately, complete error cancellation is guaranteed for the exact exchange-correlation functional, but only partial cancellation is obtained in either LDA or GGA.

Dori et al. found that the spectral distortions shown in Fig. 6a result primarily from spurious positive energy shifts of the localized σ-orbitals. They therefore hypothesized that these shifts reflect significant self-interaction errors: as the electron is spuriously repelled from itself, it is destabilized, and therefore its binding energy spuriously decreases. This error affects, in principle, all orbitals,

but self-repulsion is much more severe for the localized orbitals. As different orbitals are affected in different ways, "stretching" provides no relief in this case. Effects of a similar nature, but even greater quantitatively, were subsequently observed for metal-phthalocyanine molecules [146–148].

Körzdörfer et al. [137] proved the self-interaction error hypothesis by quantifying the per-orbital self-interaction error. Furthermore, they have shown that quantification of the self-interaction error can be used as a *predictive* criterion for the reliability of DFT calculations based on semi-local functionals: If the per-orbital self-interaction error is constant, to within the accuracy sought, then the (shifted and possibly stretched) eigenvalue spectrum will agree well with experiment. If not, the spectrum will be distorted. This quantitative criterion was successfully used by Rissner et al. to decide against the use of LDA/GGA in the theoretical study of oligopyrimidines, where experimental data were not available [149].

To summarize, simulated photoemission data, constructed from the eigenvalues of semi-local functionals, can be quantitatively useful. However, the two overwhelming deficiencies of semi-local functionals [111] – self-interaction errors and (in the standard implementation) a missing DD – limit its usefulness. Self-interaction errors restrict the application range to systems where one does not have to describe orbitals with greatly varying degrees of localization. For those systems, the missing DD requires a rigid shift of the raw data, with the general limitations of the Kohn–Sham potential typically requiring some further energy scaling of the raw data.

6.2 Self-Interaction Correction

With self-interaction being a decisive criterion for the interpretability of DFT eigenvalues, it is a natural question to ask whether one can eliminate the one-electron self-interaction error completely. A famous scheme for self-interaction correction (SIC) that achieves this has been suggested by Perdew and Zunger [62]. The basic idea is quite transparent: From a given functional approximation, here LSDA, subtract the terms that correspond to the one-electron self interaction described in the previous section:

$$E_{\mathrm{xc}}^{\mathrm{SIC}}\left[n_{\uparrow}, n_{\downarrow}\right] = E_{\mathrm{xc}}^{\mathrm{LSDA}}\left[n_{\uparrow}, n_{\downarrow}\right] - \sum_{\sigma=\uparrow,\downarrow} \sum_{i=1}^{N_{\sigma}} \left(E_{\mathrm{H}}[n_{i,\sigma}] + E_{\mathrm{xc}}^{\mathrm{LSDA}}[n_{i,\sigma}, 0]\right). \qquad (23)$$

Here, $n_{i,\sigma} = |\varphi_{i,\sigma}|^2$ are the orbital densities. The self-interaction terms are those in parenthesis on the right-hand side of (23). Several general statements can be made about the SIC that is defined in this way. For example, what are the formal grounds of this functional? It is a non-empirical, explicitly orbital-dependent (and thus an implicit) density functional. It is parameter-free and intuitively plausible. The Perdew–Zunger type correction, when used in the Kohn–Sham context, leads to

the correct $\propto -1/r$ decay of the exchange-correlation potential, and this is generally beneficial for making $-\varepsilon_{\mathrm{H}}$ closer to I. However, the correct asymptotics alone will not be enough for making $-\varepsilon_{\mathrm{H}}$ identical to I or for obtaining deeper lying eigenvalues that reflect higher ionization potentials.

Quite generally, on looking closer, there are many subtleties buried in the innocent looking (23). One should realize, e.g., that this SIC rests on identifying orbitals with electrons [150]. This immediately brings about all the caveats discussed in Sect. 5. In addition, the functional form is plausible, but there is no way of systematically improving it or expanding on it. Its intuitive plausibility can even be deceptive in some respects. For example, it has frequently been argued that the SIC of (23) would vanish when applied to the ultimate functional, because by definition the ultimate functional must be self-interaction free. Therefore, when $E_{\mathrm{xc}}^{\mathrm{LSDA}}$ in (23) would be replaced by the true, unknown exact E_{xc}, then the correction in parenthesis on the right-hand side of (23) should vanish. It has recently been pointed out [151], though, that this need not be the case: Any ground-state density functional and specifically the ultimate one is rigorously defined only on the domain of ground-state densities. Almost all many-electron system orbital densities are not ground-state densities, e.g., due to their nodal structure. Thus, strictly speaking (23) uses the ground-state energy functional with input densities that are not in the set for which the functional is defined. Furthermore, one could be tempted to use (23) as a general definition and apply it not only to LSDA but also to other functionals, e.g., GGAs. However, it has also recently been argued here that this should be avoided [152], because orbital densities are typically so different from ground-state densities that the gradient corrections that are reasonable when evaluated for ground-state densities can take unphysical values when evaluated for orbital (i.e., excited-state) densities.

The fact that makes the SIC interesting in the context of photoemission is precisely the identification of orbitals with electrons that we mentioned above. Perdew and Zunger have taken this argument to a formal level [62] and reasoned that eigenvalues from a SIC calculation should benefit from a systematic cancellation of errors. Remember that there is no formal equivalent to the original, Hartree–Fock Koopmans' in LSDA, i.e., no equality between eigenvalues and unrelaxed excitation energies. Phrased slightly differently, this means that the unrelaxed ionization energy is given by the negative of the DFT eigenvalue plus a "non-Koopmans" correction. Of course the true ionization energies include relaxation effects. Therefore, the relaxed ionization energy can be expressed as the DFT eigenvalue plus the "non-Koopmans" correction plus a relaxation energy correction. The latter correction has the opposite sign of the former. Estimating both terms for atomic densities, Perdew and Zunger showed that for LSDA the absolute value of the "non-Koopmans" correction is much larger than the relaxation correction, whereas for the SIC of (23) one can expect a reasonable cancellation between the two. Therefore, SIC eigenvalues can be good approximations to *relaxed* ionization potentials. This is a very attractive feature of the SIC, and not being tied to the

Koopmans' theorem of Hartree–Fock theory thus turns into a very powerful strength of DFT instead of a weakness.

Yet there are two reasons for being somewhat cautious about building too high expectations on these considerations. The first is that it is not clear to what extent the atom-based cancellation argument of [62] carries over to considerably more complex molecules and solids. The second is rooted in (23) itself. As the SIC energy depends on the orbitals directly, it is not straightforward to evaluate the functional derivative of (14) that yields the exchange-correlation potential. Therefore, the work of Perdew and Zunger and many SIC applications since then did not use (23) with (14), but minimized the energy with respect to the orbitals, similar to the procedure used in Hartree–Fock theory. When doing so, one has to face yet another subtlety of (23): it is not invariant under a unitary transformation of the set of occupied orbitals, i.e., different sets of occupied orbitals that yield the same density lead to different energies. As a consequence of this unitary variance problem, a direct minimization with respect to the orbitals leads to orbitals that are not orthogonal. Orthogonality can be enforced via a set of Lagrangian multipliers. This, however, leads to further questions, because with a matrix of Lagrangian multipliers $\varepsilon_{i\sigma j\sigma'}$ instead of eigenvalues $\varepsilon_{i\sigma}$, it is no longer clear which object may serve as the approximation to the ionization potential. Traditionally the eigenvalues of the matrix of Lagrange multipliers have been considered to be the equivalent of the Kohn–Sham eigenvalues [153–155]. However, it has also been argued that the eigenvalues of the matrix of Lagrange multipliers do not have any physical meaning and that the diagonal elements of this matrix correspond to the orbital energies [156]. Going deeper into the intricacies of SIC with orbital specific potentials is beyond the scope of this chapter and the reader is referred to [111, 150] for a review of different approaches to SIC. Here, we focus instead on how (23) can be related to photoemission when it is used in a Kohn–Sham context.

Equation (14) can be evaluated for explicitly orbital dependent functionals with the help of the optimized effective potential (OEP) equation [100, 111, 157–160]. The OEP combines two insights to build the local, multiplicative Kohn–Sham potential. First, the Kohn–Sham orbitals are themselves functionals of the density and, second, the functional derivative of (14) can be evaluated by using the chain rule of functional derivatives. The chain rule allows for turning the derivative of the energy with respect to the density into one with respect to the orbitals, multiplied by a derivative of the orbitals with respect to the density. The latter can be evaluated by linear response theory. A comprehensive review of OEP techniques is given in [111]. Constructing the local Kohn–Sham exchange correlation potential via the OEP approach for the SIC is numerically tedious but possible [161]. It leads to HOMO eigenvalues that often compare to first ionization potentials more favorably than those obtained from semi-local functionals. The difference between the LSDA-SIC HOMO eigenvalue and the experimental ionization potential is, e.g., 0.14 eV, 0.82 eV, and −0.27 eV for the molecules CH_4, H_2O, and CO, respectively. This is a huge improvement over LSDA, for which the corresponding values are −4.90 eV, −5.17 eV, and −6.66 eV. However, the problem with straightforward OEP calculations for the LSDA-SIC functional is that the calculations converge

very poorly – an effect that is to a considerable extent a consequence of the unitary variance problem. Therefore systematic tests or results for larger molecules are not available.

The problem can be considerably reduced by taking the unitary variance degree of freedom into account explicitly in the OEP equation. This generalized OEP (GOEP) approach allows for SIC calculations that converge much more rapidly and therefore also allow for Kohn–Sham SIC calculations for larger molecules. The theory of GOEP has been described in detail in [150]. Therefore, here we focus on the relation to photoemission. Returning to the previously mentioned small molecules reveals the drawback of going from OEP to GOEP: for CH_4, H_2O, and CO the differences between the GOEP HOMO eigenvalue and the experimental ionization potential are 1.63, 2.31, and −0.27 eV, respectively. These numbers are typical. In contrast to most other DFT approximations, which lead to eigenvalues that are too high, SIC eigenvalues are too negative, and GOEP enhances this trend over OEP. In some sense, SIC overcorrects the errors of LSDA, and thus overestimates ionization potentials.

The true strength of GOEP-SIC in practical applications thus lies not in the accurate prediction of absolute ionization energies, but in predicting orbital orderings and the relative eigenvalue spectrum, e.g., the ionization energies up to a rigid shift. The relative eigenvalue spectrum of GOEP-SIC provides, e.g., a very reasonable estimate for the upper parts of the photoemission spectrum even for "difficult" cases such as the previously discussed PTCDA molecule [137], as shown in Fig. 6b. Note that the GOEP-SIC calculation would still benefit from "stretching," for the same reasons given above, but the spectral distortion due to self-interaction errors has been removed.

A yet more notable use of GOEP-SIC has been the prediction of the intensity patterns observed in angularly resolved photoemission spectroscopy (ARPES). The relation between orbitals and ARPES can be understood based on the equations of Sect. 2. Assuming the final state $\gamma_{\mathbf{k}}$ to be a plane wave, approximating the other wavefunctions by Slater determinants, further assuming that relaxation effects are small so that initial and final Slater-determinant are built from the same set of orbitals, and taking the emission intensity as proportional to the matrix element of (4) will lead to the relation [162]

$$I\left(k_x, k_y, E_{\mathrm{kin}}\right) \propto \left|\varphi_{i\sigma}(\mathbf{k})\right|^2\Big|_{k=\mathrm{const}} \left|\mathbf{A}\cdot\mathbf{k}\right|^2. \tag{24}$$

As previously defined, $\mathbf{k}$ is the momentum of the outgoing electron (plane wave). The power of (24) lies in the observation that it builds a direct connection between the measured photoemission intensity and the Fourier transform, i.e., momentum space representation, of a molecular orbital. The factor $|\mathbf{A}\cdot\mathbf{k}|^2$ is known both experimentally and theoretically. Therefore, (24) allows for a direct comparison of theory and experiment as follows. (1) Calculate, via Fourier-transformation, the momentum representation of a molecular orbital. (2) For a given value of k, i.e., a certain kinetic energy, obtain a two-dimensional cut through the orbital (in momentum space) by plotting $\varphi_{i\sigma}(\mathbf{k})$ as a function of k_x and k_y (the value of k_z

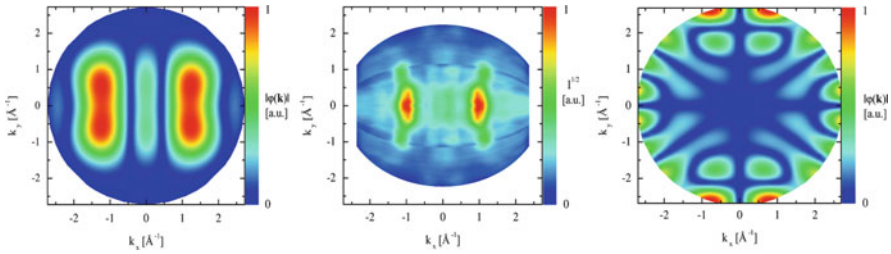

Fig. 7 *Center*: Photoemission intensity from angularly resolved photoemission spectroscopy, performed for 1,4,5,8-naphthalene-tetracarboxylic-dianhydride (NTCDA) on an Ag(110) single crystal surface, at the energy corresponding to the second ("HOMO-1") emission peak. *Left*: Cut through the momentum representation of the GOEP HOMO-1 orbital for $k = 2.73$ Å^{-1}. *Right*: Same cut for the B3LYP HOMO-1. See main text and [163] for a detailed discussion

for chosen k_x and k_y follows from the condition $k = \text{const}$) [162]. (3) According to (24), this plot is proportional to the photoemission intensity that is experimentally recorded for the same values of k_x, k_y, and k. The charming aspect of this procedure is that it allows for comparing theory and experiment in much greater detail than what one achieves by just comparing emission energies. Note, however, that ARPES measurements are not performed in the gas-phase, but typically for surface-adsorbed molecules. Because the calculation is that of a single molecule, an implicit assumption in the above procedure is that the molecule–surface interaction has negligible consequences for the electronic structure of the molecule.

Figure 7 shows in the central panel the photoemission intensity from an ARPES experiment, performed for 1,4,5,8-naphthalene-tetracarboxylic-dianhydride (NTCDA) on an Ag(110) single crystal surface with a photon energy of 36 eV (see [163] for further technical details). The color-coded intensity as a function of the momentum components k_x and k_y is shown for the second emission peak, i.e., the one that in a single-particle interpretation should correspond to the HOMO-1. The left and right panels show cuts through the HOMO-1 orbital (in momentum space) that one obtains from GOEP-SIC and from the B3LYP functional, a hybrid functional discussed at length in the next section. Clearly, the GOEP-SIC HOMO-1 momentum distribution is much closer to the experimentally observed intensity pattern than the one obtained from the B3LYP functional. Within B3LYP, there are two orbitals in close energetic vicinity, in contrast to the experiment that only observes one peak, and the orbital corresponding to the SIC HOMO-1 is the lower of the two.

From the considerations in Sects. 2 and 3 it is clear that the ARPES experiment refers to the Dyson orbital. The observation that GOEP-SIC orbitals reflect ARPES intensities indicates that these orbitals capture essential aspects of the Dyson orbitals [163] – despite the fact that the absolute accuracy of the GOEP-SIC eigenvalues is limited.

6.3 Conventional Hybrid Functionals

The next functional class we examine is that of hybrid functionals [111], pioneered by Becke [164, 165] some 20 years ago as a means of overcoming some of the remaining limitations of GGA functionals. Generally, conventional hybrid functionals incorporate a fixed *fraction* of exact-exchange energy, defined in terms of the Fock integral, given (in atomic units) by

$$E_{\mathrm{x}}^{\mathrm{exact}} = -\frac{1}{2}\sum_{\sigma=\uparrow,\downarrow}\sum_{i,j=1}^{N_\sigma}\int\int \frac{\varphi_{i,\sigma}^{*}(\mathbf{r})\varphi_{j,\sigma}^{*}(\mathbf{r}')\varphi_{j,\sigma}(\mathbf{r})\varphi_{i,\sigma}(\mathbf{r}')}{|\mathbf{r}\text{-}\mathbf{r}'|}d^3\mathbf{r}'\mathrm{d}^3\mathbf{r}, \tag{25}$$

which is familiar from Hartree–Fock theory. The exchange-correlation energy is then expressed as

$$E_{\mathrm{xc}}^{\mathrm{hyb}} = bE_x^{\mathrm{exact}} + (1-b)E_x^{\mathrm{app}} + E_c^{\mathrm{app}}, \tag{26}$$

where b is the exact-exchange fraction and the superscripts 'hyb' and 'app' denote the hybrid functional and the approximate (typically semi-local) exchange and correlation functionals from which it is constructed. As with GGA functionals, hybrid functionals can be constructed either non-empirically or semi-empirically. In the non-empirical hybrid functional based on the above-mentioned PBE GGA-functional (called PBE0 to emphasize the lack of empirical parameters) [166–168], E_x^{app} and E_c^{app} are taken from the PBE functional. Therefore b is the only free parameter and it is determined from non-empirical (though still heuristic) considerations to be 0.25 [166]. In the semi-empirical hybrid functional based on the BLYP GGA-functional, the fraction of exact exchange, as well as two additional parameters in the underlying GGA expressions, are left free and are determined by fitting to thermochemical data, leading to the functional name – B3LYP [169].

While hybrid functionals are also of growing influence in solid-state physics (see, e.g., [170, 171]), they have particularly left their mark in organic chemistry [29]. This is because they offer a further and significant reduction of errors with respect to GGA functionals. For example, for the formation enthalpies of the G3 set of thermochemical data, the mean error is 0.94 eV with PBE-GGA, but only 0.2 eV with the PBE0 hybrid functional, and 0.15 eV with B3LYP, respectively [172]. From a fundamental point of view, there are several perspectives to rationalize why one would wish to use a fraction of exact exchange, rather than all of it. One formal justification, dating back to Becke's original work [164], is grounded in the adiabatic connection theorem, the discussion of which is outside the scope of this chapter (but see [111] for an overview). For our purposes, it suffices to note that full exact exchange would necessarily require a highly non-local correlation expression, which at present is unknown. Retaining only a fraction of it provides for a reasonable balance between enjoying its advantages and retaining a simple, semi-local correlation functional.

To be used within the Kohn–Sham scheme, the exchange-correlation potential needs to be determined from the exchange-correlation energy of (26) via a functional derivative with respect to the electron density. Such derivation is certainly possible. If the orbital-dependent Fock expression is taken as an implicit functional of the density, the functional derivative can be evaluated using the OEP procedure explained in the previous section. However, this is rarely done in practice. Instead, because the Fock-exchange depends explicitly on the orbitals, the energy is derived with respect to the latter, leading to a non-local, Fock-operator potential. The name "hybrid functionals" is derived from this property, because such evaluation was originally understood to be a mixture of the Kohn–Sham and Hartree–Fock world views [164].

A more modern perspective is to view such non-local potential operators as indeed being outside the scope of the Kohn–Sham equation, but well within formal DFT nevertheless, by virtue of the *generalized* Kohn–Sham equation [173, 174]. As discussed above, the original Kohn–Sham scheme relies on the Hohenberg–Kohn theorem to establish mapping into a system that, by virtue of its non-interacting-particle nature, could be described by a single Slater determinant. In a seminal article, Seidl et al. [173] pointed out that one could equally well rely on the Hohenberg–Kohn theorem to map the real system into any interacting model system that can still be represented by a single Slater determinant, but will no longer necessarily be described by a strictly local potential. They proved that such an alternate mapping can be achieved in practice by defining an energy functional, $S[\{\varphi_i\}]$, of the orbitals $\{\varphi_i\}$ comprising the Slater determinant of the model system, and expressing the total energy as a sum of $S[\{\varphi_i\}]$, the ion–electron attraction, and a "remainder" term. One next seeks the Slater determinant that minimizes this form of the energy functional while yielding the density of the original system. The minimizing orbitals then play a role analogous to that of the Kohn–Sham orbitals. A thorough discussion of this procedure, from various perspectives, can be found in the original work of Seidl et al., as well as in several review articles [111, 112, 175]. It leads to a generalized Kohn–Sham (GKS) equation in the form

$$\left(\hat{O}^S[\{\varphi_i\}] + v_{\text{ext}}(\mathbf{r}) + v_R(\mathbf{r})\right)\varphi_j(\mathbf{r}) = \varepsilon_j\varphi_j(\mathbf{r}), \tag{27}$$

where $\hat{O}^S[\{\varphi_i\}]$ is a generally non-local, orbital-specific operator that depends on the choice of $S[\cdot]$ but not on the system specifics, and

$$v_R(\mathbf{r}) \equiv \frac{\delta R^S[n]}{\delta n(\mathbf{r})} \tag{28}$$

is the "remainder potential," a multiplicative potential which is a functional of the density, that is determined from a functional derivative of a "remainder" energy term, $R^S[n]$.

Formally, both the KS and the GKS maps are exact [173]. However, whereas there is only one KS map, there exist a multitude of GKS maps, depending on the

choice of $S\,[\{\varphi_i\}]$. If one chooses $S\,[\{\varphi_i\}]$ to be the kinetic energy of the fictitious system, then $\hat{O}^S\,[\{\varphi_i\}]$ is simply the usual single-particle kinetic energy operator, i.e., the first term in the KS equation. The "remainder" potential, $v_R(\mathbf{r})$, is then simply the sum of the Hartree and exchange-correlation terms of the KS equation, and the KS and GKS equations are one and the same. However, if one chooses $S\,[\{\varphi_i\}]$ to be the Slater determinant expectation value of the sum of the kinetic energy and a *fraction b* of the electron-repulsion energy operator, then $\hat{O}^S\,[\{\varphi_i\}]$ is the kinetic energy operator, together with a fraction b of the Fock operator and the same fraction b of the Hartree term. From this point of view, if one chooses the rest of the Hartree term, the fraction $1\text{-}b$ of the semi-local exchange potential, and the semi-local correlation potential, as the approximate $v_R(\mathbf{r})$, one obtains exactly the "hybrid" combination of local and non-local potentials corresponding to the energy expression of (26) [112]. Thus, while the name hybrid functional persists for historical reasons, and we too use it here, there is nothing that is intrinsically "hybrid" about hybrid functionals [111, 112, 174, 175].

Just like LDA and GGA functionals, hybrid functionals were not developed with quasi-particle considerations in mind. It is therefore instructive to examine whether, and the extent to which, they improve on the description of photoemission afforded by semi-local functionals. Specifically, can hybrid functionals reduce the need for a "shift and stretch" procedure and the difficulties of describing systems with both localized and delocalized states? And if so, to what extent?

Let us start answering these questions by considering the necessity of a rigid shift of the eigenvalue spectrum. Given the exact "remainder" functional, the ionization potential (Koopmans') theorem of (20) is as valid for the exact GKS framework as it is for the exact KS framework [112, 174]. In practice, the GKS "remainder" potential, just like the exchange-correlation KS potential, can exhibit a derivative discontinuity (DD) [112, 176]. Its absence in the approximate remainder potential associated with the conventional hybrid functional will cause a departure of $-\varepsilon_{\mathrm{H}}$ from I, just as with the semi-local functionals. Remember, however, that the DD in the exchange-correlation potential is there to "absorb" whatever discontinuity of the chemical potential is not reflected in the kinetic energy term (see Sect. 5). In the GKS equation, some of this burden is shouldered by the other non-local terms, i.e., the Fock one in our case. Thus, it can be expected quite generally that the missing DD in a hybrid functional would be smaller [111, 173, 174, 177].

This expectation is indeed borne out by considering again our two prototypical molecules – pentacene and PTCDA. For both molecules the semi-local PBE functional $-\varepsilon_{\mathrm{H}}$ differs from I as calculated from total energy differences by ~1.75 eV. With the semi-local PBE0 functional, this differences reduce to ~1.2 eV. However, the remaining difference is still far too large for the eigenvalues to be useful as they are. Therefore a rigid shift of precisely the type discussed in Sect. 6.1 is still needed and hybrid functionals are not truly helpful in this respect. Similar conclusions are drawn even when inspecting a wider set of reference molecules (see, e.g., [178, 179]).

Turning to the rest of the outer-valence electron spectrum, what is the effect of the fraction of exact exchange? For pentacene, Fig. 5b shows the (appropriately

shifted) eigenvalue spectrum obtained with the B3LYP and PBE0 hybrid functionals [135, 136]. For this system, where the shifted spectrum from the PBE functional already provided a qualitatively useful answer, the hybrid functional spectrum provides further improvement by essentially eliminating the need for a "stretch factor." We emphasize strongly that this is a direct consequence of using the GKS approach, i.e., a non-local Fock-operator potential. To prove that, Fig. 5b also shows the spectrum obtained from the B3LYP functional, but with a KS potential obtained from solving the OEP equation [135]. Clearly, these results do need stretching, despite the underlying use of hybrid functional energy expression, and are in fact quite similar to those obtained with PBE-GGA.

Körzdörfer and Kümmel rationalized the stretching afforded by using the GKS procedure [135]. They argued that, if the differences in the KS and GKS orbitals are ignored, then the difference between each GKS and corresponding KS eigenvalue can be viewed in terms of first-order perturbation theory involving the difference between the Fock and semi-local exchange. They suggested that this first-order correction mimics successfully the above-mentioned first-order correction between Kohn–Sham values and ionization energies due to Chong et al. [103]. We note that the hybrid first-order correction only involves a term related to fractional non-local exchange, whereas the Chong et al. correction involves a non-local exchange term as well as a correlation term. However, using only a fraction of Fock exchange so as to affect a reasonable balance between exchange and correlation is precisely the rationale of the hybrid functional. Indeed, if the photoemission spectrum of a hybrid functional is studied as a function of the Fock fraction b, it is discovered that the standard fraction, conceived in the design of the functional from energetic considerations is also best for the photoemission spectrum [135, 180]. A different, complementary perspective for the improved "stretch" afforded by the hybrid functional calculation is that the non-local potential is more likely to mimic well the self-energy operator, which is itself non-local [111, 112, 173, 181, 182]. While the non-local potential still cannot be equivalent to the self-energy operator, as it is not frequency-dependent, it certainly constitutes a step in the right direction.

An even more dramatic improvement of hybrid functionals, employed using the GKS scheme, over semi-local ones is found for our second prototypical system – PTCDA – as shown in Fig. 6b. Clearly, the spectral distortion is strongly reduced. In particular, the leading spurious peak obtained from the PBE-GGA calculation is gone and eigenvalues of localized states, spuriously pushed too high by the GGA calculation, are returned to lower energies where their resemblance to experimental and/or *GW* data is greatly improved. Again, this improvement is not fully obtained if one employs the hybrid functional using the OEP procedure, as also shown in Fig. 6b. Not only is "stretching" needed with the OEP procedure, as explained above, but in fact some of the desirable orbital ordering is lost. A similar improvement of conventional hybrid functionals over semi-local ones has been repeatedly found for porphyrins and phthalocyanins – a different class of prototypical molecules comprising both localized and delocalized states; see, e.g., [147, 148, 180, 183–185]. For such systems, highly detailed comparisons to sufficiently-resolved experimental data often reveal that some further quantitative improvement can be

obtained from a *GW* calculation (see, e.g., [186, 187]). Nevertheless, the degree of quantitative agreement between the conventional hybrid spectrum and the *GW* spectrum is often as good as the experimental resolution.

This success of the hybrid functional approach is not at all a trivial finding: we have argued above that these distortions result from self-interaction errors, but hybrid functionals are certainly not self-interaction free! Complete cancellation of the self-interaction in the Hartree term would require the full Fock exchange, not just a fraction of it, along with a self-interaction free correlation potential. Neither condition is met in a conventional hybrid functional. One can only conclude that again a reasonable balance between exchange and correlation is struck by using a fraction of Fock exchange. While this balance cannot and does not eliminate self-interaction errors (as also obvious from the results of Fig. 7 and the above discussion), it does mitigate them to a point where the eigenvalue spectrum more closely resembles the spectrum obtained from many-body perturbation theory, to the point where quantitative or close-to-quantitative agreement of the shifted eigenvalue spectrum with experiment is often found.

To summarize, conventional hybrid functionals differ from semi-local ones not only in the form of the exchange-correlation energy but also in that they are usually evaluated using a non-local potential operator within the generalized Kohn–Sham scheme. These two differences reduce, but far from eliminate, the need for a rigid shift of the eigenvalue spectrum. They do mitigate very strongly, often quantitatively, the need for spectral "stretching" and the distortions arising from self-interaction errors.

6.4 Range-Separated Hybrid Functionals

A disadvantage that is common to all preceding classes of functionals is the incorrect prediction of the ionization potential, I, as well as the electron affinity, A. For gas-phase systems, we have already mentioned that these quantities can easily be calculated from total energy differences. Therefore one could argue that obtaining an eigenvalue spectrum that is similar to photoemission data, up to a rigid shift (as with the self-interaction-corrected or hybrid functionals of the preceding two sections), is quite sufficient. However, significant further advantages can be gained if indeed I and A can be equated with $-\varepsilon_{\mathrm{H}}$ and $-\varepsilon_{\mathrm{L}}$, respectively. For example, accurate positioning of frontier orbitals is essential for transport calculations and therefore gross errors in the calculation of conductance can ensue from the use of approximate DFT forms [188–190]. More importantly for the gas phase, if we are truly to mimic the results of many-body perturbation theory with DFT, one would prefer to retain, if possible, an intuitive connection between single-particle energy levels and quasi-particle excitations. This is especially so if one also wishes to consider optical excitations, which can be thought of as simultaneous excitation of a quasi-electron and a quasi-hole [44, 191]. Obtaining the correct fundamental gap is in fact crucial for describing the electron–hole interaction in terms of an

exciton binding energy, as one does in many-body perturbation theory [112] and in particular indispensable for the description of charge transfer excitations using linear-response within TDDFT [192–196].

We have already explained in Sect. 5 that equating $-\varepsilon_{\mathrm{L}}$ with A is not possible within the Kohn–Sham scheme owing to the usually non-negligible DD. We have also argued in Sect. 6.3 that within the generalized Kohn–Sham scheme there is hope for reducing the magnitude of the DD, but that in practice conventional hybrid functionals do not achieve this lofty goal. Stein et al. [197] observed that in the gas phase the asymptotic potential must play a crucial role in the energetics of electron addition and removal. However, an asymptotically correct $1/r$ Coulomb potential is obtained only if the full Fock exchange cancels out the self-interaction in the Hartree term. As explained in Sect. 6.3, in conventional hybrid functionals only a fraction of the Fock exchange is used. Increasing that fraction would disrupt the hard-earned and delicate balanced between exchange and correlation. In order to escape this conundrum, then, we must step out of the conventional hybrid functional framework.

One appealing idea is the range-separated hybrid (RSH) functional, proposed by Savin and co-workers [198]. In the simplest realization of this idea, the repulsive Coulomb potential is split into a long-range (LR) and short-range (SR) term, e.g., via

$$1/r = \mathrm{erf}(\gamma r)/r + \mathrm{erfc}(\gamma r)/r, \tag{29}$$

where $\mathrm{erf}(\cdot)$ and $\mathrm{erfc}(\cdot)$ denote the standard and complementary error functions, respectively, and γ is a range-separation parameter. The SR and LR components are taken together in the usual way for the Hartree term, yielding the standard Hartree potential, but the components are treated differently in the generation of the exchange term. The LR part is treated via a Fock exchange term, but the SR part is treated using semi-local exchange. A conventional semi-local correlation expression is used throughout. Minimization of the ensuing exchange-correlation energy expression with respect to orbitals then leads to

$$\left(-\frac{\nabla^2}{2} + v_{\mathrm{ext}}(\mathbf{r}) + v_{\mathrm{H}}([n];\mathbf{r}) + \hat{v}_{\mathrm{F}}^{\mathrm{lr},\gamma} + v_x^{\mathrm{sr},\gamma}([n];\mathbf{r}) + v_c^{\mathrm{sl}}([n];\mathbf{r})\right)\varphi_i(\mathbf{r}) = \varepsilon_i\varphi_i(\mathbf{r}), \tag{30}$$

where $\hat{v}_{\mathrm{F}}^{\mathrm{lr},\gamma}$ is a long-range Fock-like operator, namely

$$\hat{v}_{\mathrm{F}}^{\mathrm{lr},\gamma}\varphi_i(\mathbf{r}) = -\sum_j \varphi_j(\mathbf{r}) \int d\mathbf{r}' \frac{\mathrm{erf}\left(\gamma\left|\mathbf{r}-\mathbf{r}'\right|\right)}{\left|\mathbf{r}-\mathbf{r}'\right|}\varphi_j^*(\mathbf{r}')\varphi_i(\mathbf{r}'), \tag{31}$$

$v_x^{\mathrm{sr},\gamma}([n];\mathbf{r})$ is the multiplicative potential arising from the semi-local treatment of the SR exchange, and $v_c^{\mathrm{sl}}([n];\mathbf{r})$ is the (multiplicative) correlation potential. The logic of the range-separation idea (which is rooted in even earlier efforts to wed DFT with the configuration-interaction method [199, 200]) is that the relative

importance of exchange and correlation is different for different interaction ranges. Our above quandary of the two seemingly contradictory requirements is solved, then, by "partition of labor." The exact LR Fock exchange is in charge of enforcing the correct form of the asymptotic potential. At the same time, the semi-local SR exchange is in charge of maintaining the delicate balance with correlation.

It is readily established that the RSH construct of (30) is yet another special case of the generalized Kohn–Sham approach [112]. To show that, we choose $S[\{\varphi_i\}]$ to be the Slater-determinant expectation value of the sum of the kinetic energy and the long-range electron-repulsion energy operator, $\mathrm{erf}(\gamma r)/r$. This yields the usual kinetic energy operator, together with the LR fraction of the Fock operator and the Hartree term. Our specific choice of the "remainder potential," $\nu_R(\mathbf{r})$, is then the sum of the SR Hartree term, the local potential derived from the SR exchange term, and a standard correlation potential.

In order to use the RSH scheme, one must still decide on the choice for the range-separation parameter, γ. Physically, $1/\gamma$ can be viewed as the range below which the exchange is dominated by its SR contribution and above which the exchange is dominated by its LR contribution. To realize that the choice of γ plays a crucial role in the success of the approach, it suffices to consider its limits. For $\gamma \to 0$, (30) reduces to the usual Kohn–Sham equation (12), with a semi-local functional. For $\gamma \to \infty$, it reduces to the Hartree–Fock equation with added semi-local correlation. The former has already been noted to underestimate the fundamental gap severely and the latter is well-known to overestimate it severely [111]. How can we tell, then, in a predictive manner, which values of γ we should choose to use?

Clearly, just as in some semi-local functionals and conventional hybrid functionals, one can opt to proceed semi-empirically. This means that γ, possibly together with other free parameters in the semi-local exchange and correlation terms, can be fitted based on appropriate reference data. In fact, most modern RSH functionals are constructed in this way – see, e.g., [201–207]. However, both formal considerations [208] and practical simulations for the homogeneous electron gas problem [209] show that obtaining accurate results often requires significantly different values of γ. In fact, γ itself can be viewed as functional of the density [208], on which very little is known.

Within the range-separated hybrid functional approach, an essential concept for overcoming this difficulty is the use of non-empirical, system-specific optimal tuning to determine the range separation parameter. This allows us to overcome the absence of a universal, system-independent value for the range-separation parameter, γ. For photoemission, one would like to identify the HOMO orbital with the ionization potential, i.e., to uphold the ionization potential theorem of (20), $-\varepsilon_{\mathrm{H}} = I$. Therefore, one can employ the concept of optimal tuning in practice by actively seeking the value of γ for which (20) is obeyed [209]. This means that we seek γ for which the negative of the HOMO energy is the same as the ionization potential determined from the total energy difference between cation and neutral. This approach was indeed found to be very successful in the prediction of ionization

potentials for gas-phase objects – see, e.g., [112, 175, 179, 193, 197, 210]. Using an RSH functional whose semi-local correlation and SR semi-local exchange are based on the PBE functional, for our prototypical molecules of pentacene and PTCDA, this yields HOMO values that differ from the experimental ionization potentials value by only ~0.2 eV [136]. This indicates that an accuracy on par with that of *GW* is, in fact, possible with a suitably-constructed functional.

As mentioned above, for applications such as transport or optical excitations, it is also important to equate the LUMO with the electron affinity, A. Because the exact remainder potential of the GKS approach, $v_R(\mathbf{r})$, may possess a derivative discontinuity, an analogous ionization potential theorem that relates the LUMO energy to the electron affinity does not exist. However, this problem can be circumvented by considering, instead, I of the N+1 electron system which (barring relaxation effects that we do not allow) is the same as A of the N-electron system. We can therefore seek γ that obeys the ionization potential theorem for both N and $N + 1$ electron systems as closely as possible [193, 197], e.g., in a least squares sense. In other words, one can seek γ that minimizes a target function, $J(\gamma)$, given by

$$J^2(\gamma) = \left(\varepsilon^{\gamma}_{\mathrm{H}(N)} + I^{\gamma}_{N}\right)^2 + \left(\varepsilon^{\gamma}_{\mathrm{H}(N+1)} + I^{\gamma}_{N+1}\right)^2 \tag{32}$$

(for related tuning criteria, see, e.g., [194, 211]). Stein et al. [197] have shown that use of an RSH functional with optimal tuning based on (32) yields generalized Kohn–Sham HOMO–LUMO gaps that are in excellent quantitative agreement with experiment for a range of atoms, molecules, and clusters. Thus, the myth that DFT can never yield reliable, non-empirical predictions for fundamental gap values was dispelled. HOMO-LUMO gaps of similar quality, for a variety of gas-phase objects, have since been reported by several groups – see, e.g., [179, 196, 212–215] (with numerous additional successful applications to charge transfer excitations that are outside the scope of this chapter, but see [112] for a recent overview). Specifically for pentacene and PTCDA, this procedure yields HOMO–LUMO gaps that are within ~0.1 eV from *GW* values [136].[1]

Briefly, the optimal tuning approach succeeds because conditions such as those of (20) or (32) assist in choosing, from all possible GKS maps in the form of (30), the one which minimizes the role of the derivative discontinuity [112, 197]. Furthermore, Stein et al. have recently proven that, generally, a missing derivative discontinuity and deviation from piecewise linearity in the ensemble treatment of fractional-electron DFT (see Sect. 6.1) are in fact doppelgänger: they must appear or disappear simultaneously and they are quantitatively equivalent [176]. Indeed, much recent work, especially from the group of Autschbach, has shown explicitly that optimal tuning also minimizes deviations from piecewise linearity for the

[1] Here the comparison is to the HOMO–LUMO gap obtained from a G_1W_1 calculation, where the G_0W_0 calculation is used as the starting point for constructing G and W for a subsequent GW calculation. This approach has been found in [51] to provide a HOMO–LUMO gap for molecular pentacene that is in excellent agreement with experiment.

[$N-1$,N] and [N,$N+1$] segments – see, e.g., [112, 136, 176, 216–220]. We note in passing that correction terms that enforce piecewise linearity offer a different, but somewhat related, approach to improving the correspondence of DFT HOMO to the ionization potential [221–226], which may also be applied to improving the correspondence of lower-lying eigenvalues to photoemission results. Its detailed discussion is outside the scope of the present work, but the interested reader is referred to the above references for a thorough discussion.

Importantly, the optimal tuning idea is more than just a successful mathematical device. Fundamentally, it can be viewed as a significant departure from the usual paradigm for functional construction and application, in which one seeks an increasingly general functional form that can come as close as possible to the ideal of a universal functional. Instead, the notion of an all-purpose functional expression is sacrificed so as to gain greatly in simplicity and applicability with no loss of accuracy [112]. From this perspective, range-separated hybrid functionals can be thought of as a special case of a new, "fourth generation" class of functionals, which are not and cannot be expressed explicitly, but are defined implicitly via a numerical procedure [211].

The quality of the photoemission spectra obtained from this approach has been studied by Refaely-Abramson et al. [136]. Returning to the pentacene example of Fig. 5b, we find that the above procedure is indeed sufficient to retain the quantitative accuracy of the outer-valence photoemission spectrum, achieved with the SIC or conventional hybrid approaches, while eliminating the need for a rigid shift. Therefore, the accuracy of many-body perturbation theory is matched throughout. Note, however, that as with all the other above-surveyed functionals, this level of agreement is expected to (and does) gradually deteriorate for deeper excitations – see the discussion in Sect. 5 and especially Fig. 3. Again, this can be partly offset with a milder stretch factor.

For PTCDA (Fig. 6b), the picture is again more complicated. While the optimally-tuned RSH approach succeeds in eliminating the need for a rigid shift, the largely successful description of the energy position of localized states, obtained with SIC, conventional hybrids, and of course *GW*, is not fully achieved. The situation is not as dire as with LDA or GGA, but is not satisfactory either. Refaely-Abramson et al. [136] argued that this limitation arises from the lack of a sufficient amount of non-local exchange in the short-range. Recall that, by construction, the approach of (29) and (30) suppresses Fock-exchange in the short-range, whereas with a conventional hybrid functional, as in (26), non-local Fock exchange exists throughout. It also stands to reason that, for strongly localized orbitals, the long-range potential is not strongly felt and it is the short-range component of the non-local Fock exchange that is more important for mitigation of self-interaction errors [147].

The importance of SR non-local exchange is confirmed by considering a different kind of range-separated functional – the Heyd–Scuseria–Ernzerhof functional [227, 228]. HSE is similar to the conventional hybrid functional PBE0 in the short range, in that it possesses the same fraction of non-local exchange, but unlike PBE0 it does not contain any non-local exchange in the long-range (and therefore does not

obtain the correct asymptotic potential and disobeys (20) [112]). Marom et al. [147] have studied the copper phthalocyanine (CuPc) molecule and have shown that, aside from a different rigid shift, the HSE eigenvalue spectrum is virtually identical to that obtained from a conventional hybrid functional. By mitigating the self-interaction error equally well, HSE is just as useful as a conventional hybrid functional in generating sufficiently quantitative agreement with experiment – an observation confirmed since for a variety of molecular systems – see, e.g., [149, 229–233].

Refaely-Abramson et al. argued that LR Fock exchange, crucial for obtaining the ionization potential, can be combined seamlessly with a fraction of SR Fock exchange, crucial for the mitigation of self-interaction errors, by starting with the more general Coulomb partition expression of Yanai et al. [202], given by

$$\frac{1}{r} = \frac{\alpha + \beta \mathrm{erf}(\gamma r)}{r} + \frac{1 - [\alpha + \beta \mathrm{erf}(\gamma r)]}{r}. \tag{33}$$

The first term is then treated in a Fock-like manner, whereas the second term is treated using semi-local exchange (even more general range-separation schemes can be devised, e.g., to include a middle range as well; see, e.g., [234]). Here, γ is the range-separation parameter as before, but the additional parameters α and β control the fraction of the non-local exchange term, which tends to α for $r \to 0$ and to $\alpha + \beta$ for $r \to \infty$. Therefore, choosing $\beta = 1 - \alpha$ guarantees the correct asymptotic potential while retaining a desired fraction α in the short range [136, 216]. γ can be determined from tuning considerations similar to those employed in (30). In some cases α can itself be determined from first principles based on piecewise-linearity arguments [136, 216]. When using PBE-based semi-local exchange and correlation components, α is usually found to be ~0.2, which is in fact the recommended semi-empirical value based on fitting of thermochemical data [207]. As shown in Fig. 6b, this does indeed offer further meaningful improvement on the simpler optimally-tuned RSH functional and its results are in essentially quantitative agreement with *GW*. We note that inclusion of SR exchange does not necessarily result in piecewise linearity for highly charged species of the studied system [235]. However, while indeed piecewise linearity in principle should be observed with the exact functional also for highly charged species, it is not necessary for an accurate description of the photoemission process, which has to do with excited states of the singly-charged cation [236].

Naturally, optimally-tuned RSH functionals are not a panacea. They are not as accurate for deeper-lying orbitals, are not fully self-interaction free, do not address non-local correlation effects, may be problematic for larger systems [237], and are difficult to generalize to solid-state or heterogeneous systems [112]. Nevertheless, they can offer an outer-valence photoemission spectrum, as well as a fundamental gap, of quality comparable to that of many-body perturbation theory in the *GW* approximation, which is no small feat for a DFT-based approach.

7 Conclusions

In this chapter, we have attempted to portray challenges and progress made with the application of density functional theory to the simulation of gas-phase outer-valence photoemission spectra. After a brief explanation of photoemission spectroscopy, we discussed how it should be viewed theoretically from a many-electron wave function approach and from a many-body perturbation theory approach. We then discussed how photoemission should be approached within time-dependent DFT, a rigorous excited-state theory, and also how it can be understood approximately using the single-electron energies and orbitals of ground state DFT. Finally, we examined the achievements made, and the difficulties remaining, with classes of approximate functionals, using prototypical molecular systems as benchmark cases for practical performance.

We end this chapter with two comments. First, we have discussed numerous instances where DFT calculations can go wrong and indeed we feel that, as in experimental work, one must be deeply familiar with the inner workings of the methods employed in order to avoid artifacts. Nevertheless, we would like to stress very strongly that our message is not at all one of disappointment, but in fact one of optimism. As we have explained throughout, recent years have seen significant progress in understanding potential pitfalls in the application of DFT to photoemission and in developing successful methods to overcome them. Consequently, many applications once considered to be "too difficult for DFT" are now well within our reach. Second, the examples we have selected for this tutorial overview were, quite naturally, strongly biased towards the (joint and separate) research work of the authors. Unfortunately, within the confines of this chapter it would be impossible to do full justice to the all work of many other scientists on a great variety of additional systems. Nevertheless, we do believe that the work surveyed here provides some general lessons and perspectives. We therefore hope it will be of benefit to scientists working in this fascinating area.

Acknowledgements We thank Roi Baer (Hebrew University, Jerusalem) for a very large number of illuminating discussions, as part of joint work discussed throughout this chapter. We also thank Reut Baer (second grade student, Yeffe Nof Elementary School, Jerusalem) for her artistic work on Fig. 1a. We thank Sivan Refaely-Abramson and Matthias Dauth for helpful discussions, and Sivan Refaely-Abramson for preparing Figs. 5 and 6. Work in Rehovoth was supported by the European Research Council, the Israel Science Foundation, the German-Israeli Foundation, the Leona M. and Harry B. Helmsley Charitable Trust, the Wolfson Foundation, and the Lise Meitner Center for Computational Chemistry. Work in Bayreuth was supported by the German-Israeli Foundation, by Deutsche Forschungsgemeinschaft GRK 1640, by the Bavarian State Ministry of Science, Research, and by the Arts for the Collaborative Research Network "Solar Technologies go Hybrid".

References

1. Hüfner S (2010) Photoelectron spectroscopy: principles and applications. Springer, Berlin
2. Briggs D, Seah MP (eds) (1990) Practical surface analysis, Auger and X-ray photoelectron spectroscopy, 2nd edn. Wiley, New York
3. Woodruff DP, Delchar AT (1994) Modern techniques of surface science, 2nd edn. Cambridge University Press, Cambridge
4. Hertz H (1887) Über einen einfluss des ultravioletten lichtes auf die electrische entladung. Ann Phys 267:983
5. Einstein A (1905) Zur elektrodynamik ewegter körper. Ann Phys 17:891
6. Hendrickson DN, Hollander JM, Jolly WL (1969) Nitrogen 1s electron binding energies. Correlations with molecular orbital calculated nitrogen charges. Inorg Chem 8:2642
7. Evans S, Orchard AF (1970) The Helium-(I) photoelectron spectra of some halogens and diatomic interhalogens. Inorg Chim Acta 5:81
8. Turner DW, Al Jobory MI (1962) Determination of ionization potentials by photoelectron energy measurement. J Chem Phys 37:3007
9. Jellinek J (ed) (1999) Theory of atomic and molecular clusters: with a glimpse at experiments. Springer, Berlin
10. Khanna SN, Castleman AW (eds) (2007) Quantum phenomena in clusters and nanostructures. Springer, Berlin
11. Kawazoe Y, Kondow T, Ohno K (eds) (2009) Clusters and nanomaterials: theory and experiment. Springer, Berlin
12. Eberhardt W (2002) Clusters as new materials. Surf Sci 500:242
13. Kroto HW, Heath JR, O'Brian SC, Curl RF, Smalley RE (1985) C60: buckminsterfullerene. Nature 318:162
14. Kroto HW (1992) C60: buckminsterfullerene, the celestial sphere that fell to Earth. Angew Chem 31:111
15. Cheshnovsky O, Yang SH, Pettiette CL, Craycraft MJ, Smalley RE (1987) Ultraviolet photoelectron spectroscopy of semiconductor clusters: silicon and germanium. Chem Phys Lett 138:119
16. Yang S, Taylor KJ, Craycraft MJ, Conciecao J, Pettiertte CL, Cheshnovsky O, Smalley RE (1988) UPS of 230-atom carbon C: chains and rings. Chem Phys Lett 144:431
17. Taylor KJ, Pettiette-Hall CL, Cheshnovsky O, Smalley RE (1992) Ultraviolet photoelectron spectra of coinage metal clusters. J Chem Phys 96:3319
18. Klauk H (ed) (2006) Organic electronics: materials, manufacturing, and applications. Wiley-VCH, Hoboken
19. Klauk H (ed) (2012) Organic electronics II: more materials and applications. Wiley-VCH, Hoboken
20. Sato N, Seki K, Inokuchi H (1981) Polarization energies of organic solids determined by ultraviolet photoelectron spectroscopy. J Chem Soc Faraday Trans 2 77:1621
21. Liebsch T, Plotzke O, Heiser F, Hergenhahn U, Hemmers O, Wehlitz R, Viefhous J, Langer B, Whitfield SB, Becker U (1995) Angle-resolved photoelectron spectroscopy of C_{60}. Phys Rev A 52:547
22. Fukagawa H, Yamane H, Kataoka T, Kera S, Nakamura M, Kudo K, Ueno N (2006) Origin of the highest occupied band position in pentacene films from ultraviolet photoelectron spectroscopy: hole stabilization versus band dispersion. Phys Rev B 73:245310
23. Dori N, Menon M, Kilian L, Sokolowski M, Kronik L, Umbach E (2006) Valence electronic structure of gas phase 3,4,9,10-perylene tetracarboxylic-acid-dianhydride (PTCDA): experiment and theory. Phys Rev B 73:195208
24. Evangelista F, Carravetta V, Stefani G, Jansik B, Alagia M, Stranges S, Ruocco A (2007) Electronic structure of copper phthalocyanine: an experimental and theoretical study of occupied and unoccupied levels. J Chem Phys 126:124709

25. Akaike K, Kanai K, Yoshida H, Tsutsumi J, Nishi T, Sato N, Ouchi Y, Seki K (2008) Ultraviolet photoelectron spectroscopy and inverse photoemission spectroscopy of [6,6]-phenyl-C_{61}-butyric acid methyl ester in gas and solid phases. J Appl Phys 104:023710
26. Sauther J, Wüsten J, Lach S, Ziegler C (2009) Gas phase and bulk ultraviolet photoemission spectroscopy of 3,4,9,10-perylene-tetracarboxylic dianhydride, 1,4,5,8-naphthalenetetracarboxylic dianhydride, and 1,8-naphthalene-dicarboxylic anhydride. J Chem Phys 131:034711
27. Parr RG, Yang W (1989) Density functional theory of atoms and molecules. Oxford University Press, Oxford
28. Gross EKU, Dreizler RM (1990) Density functional theory: an approach to the quantum many-body problem. Springer, Berlin
29. Koch W, Holthausen MC (2001) A chemist's guide to density functional theory. Wiley, Heidelberg
30. Fiolhais C, Nogueira F, Marques MAL (eds) (2003) A primer in density functional theory, vol 620, Lectures in Physics. Springer, Berlin
31. Capelle K (2006) A bird's-eye view of density-functional theory. Braz J Phys 36:1318
32. Sholl DS, Steckel JA (2009) Density functional theory: a practical introduction. Wiley, Hoboken
33. Engel E, Dreizler R (2011) Density functional theory: an advanced course. Springer, Berlin
34. Burke K, Wagner LO (2013) DFT in a nutshell. Int J Quant Chem 113:96
35. Martin RM (2004) Electronic structure: basic theory and practical methods. Cambridge University Press, Cambridge
36. Walter M, Häkkinen H (2008) Photoelectron spectra from first principles: from the many-body to the single-particle picture. New J Phys 10:043018
37. Dauth M, Wiessner M, Schöll A, Puschnig P, Reinert F, Kümmel S (2014) Angular resolved photoemission from organic semiconductors: orbital imaging beyond the molecular orbital interpretation (unpublished)
38. Landau LD (1957) The theory of a Fermi liquid. Sov Phys JETP 3:920
39. Hedin L (1965) New method for calculating the one-particle Green's function with application to the electron-gas problem. Phys Rev 139:A796
40. Hybertsen MS, Louie SG (1986) Electron correlation in semiconductors and insulators: band gaps and quasiparticle energies. Phys Rev B 34:5390
41. Aryasetiawan F, Gunnarsson O (1998) The GW method. Rep Prog Phys 61:237
42. Aulbur WG, Jönsson L, Wilkins JW (1999) Quasiparticle calculations in solids. Solid State Phys 54:1
43. Hedin L (1999) On correlation effects in electron spectroscopies and the GW approximation. J Phys Condens Matter 11:R489
44. Onida G, Reining L, Rubio A (2002) Electronic excitations: density-functional versus many-body Green's functions approaches. Rev Mod Phys 74:601
45. Gross EKU, Runge E, Heinonen O (1991) Many-particle theory. IOP Publishing, Bristol
46. Grossman JC, Rohlfing M, Mitas L, Louie SG, Cohen ML (2001) High accuracy many-body calculational approaches for excitations in molecules. Phys Rev Lett 86:472
47. Chelikowsky JR, Kronik L, Vasiliev I (2003) Time-dependent density-functional calculations for the optical spectra of molecules, clusters, and nanocrystals. J Phys Condens Matter 15: R1517
48. Makmal A, Armiento R, Engel E, Kronik L, Kümmel S (2009) Examining the role of pseudopotentials in exact-exchange-based Kohn-Sham Gaps. Phys Rev B 80:161204(R)
49. Sai N, Tiago ML, Chelikowsky JR, Reboredo FA (2008) Optical spectra and exchange-correlation effects in molecular crystals. Phys Rev B 77:161306
50. Blase X, Attaccalite C (2011) Charge-transfer excitations in molecular donor-acceptor complexes within the many-body Bethe-Salpeter approach. Appl Phys Lett 99:171909
51. Sharifzadeh S, Biller A, Kronik L, Neaton JB (2012) Quasiparticle and optical spectroscopy of the organic semiconductors pentacene and PTCDA from first principles. Phys Rev B 85:125307

52. Rohlfing M, Louie SG (1998) Excitonic effects and optical absorption spectrum of hydrogenated Si clusters. Phys Rev Lett 80:3320
53. Rohlfing M, Louie SG (2000) Electron-hole excitations and optical spectra from first principles. Phys Rev B 62:4927
54. Tiago ML, Chelikowsky JR (2006) Optical excitations in organic molecules, clusters, and defects studied by first-principles greens function methods. Phys Rev B 73:205334
55. Rocca D, Lu D, Galli G (2010) Ab initio calculations of optical absorption spectra: solution of the Bethe-Salpeter equation within density matrix perturbation theory. J Chem Phys 133:164109
56. Hohenberg P, Kohn W (1964) Inhomogeneous electron gas. Phys Rev 136:B864
57. Kohn W, Sham L (1965) Self-consistent equations including exchange and correlation effects. J Phys Rev 140:A1133
58. von Barth U, Hedin L (1972) A local exchange-correlation potential for the spin polarized case: I. J Phys C Solid State Phys 5:1629
59. Rajagopal AK, Callaway J (1973) Inhomogeneous electron gas. Phys Rev B 7:1912
60. Ceperley DM, Alder BJ (1980) Ground state of the electron gas by a stochastic method. Phys Rev Lett 45:566
61. Vosko SJ, Wilk L, Nusair M (1980) Accurate spin-dependent electron liquid correlation energies for local spin density calculations: a critical analysis. Can J Phys 58:1200
62. Perdew JP, Zunger A (1981) Self-interaction correction to density-functional approximations for many-electron systems. Phys Rev B 23:5048
63. Perdew JP, Wang Y (1992) Accurate and simple analytic representation of the electron-gas correlation energy. Phys Rev B 45:13244
64. Yin MT, Cohen ML (1980) Microscopic theory of the phase transformation and lattice dynamics of Si. Phys Rev Lett 45:1004
65. Marques MAL, Maitra NT, Noqueira FMS, Gross EKU, Rubio A (eds) (2012) Fundamentals of time-dependent density functional theory, vol 837, Lecture Notes in Physics. Springer, Berlin
66. Ullrich C (2012) Time-dependent density-functional theory: concepts and applications. Oxford University Press, Oxford
67. Burke K, Werschnik J, Gross EKU (2005) Time-dependent density functional theory: past, present, and future. J Chem Phys 123:062206
68. Baer R, Kronik L, Kümmel S (eds) (2011) Special issue on 'open problems and new solutions in time-dependent density functional theory'. Chem Phys 391:1–176
69. Runge E, Gross EKU (1984) Density-functional theory for time-dependent systems. Phys Rev Lett 52:997
70. Mundt M, Kümmel S (2005) Derivative discontinuities in time-dependent density-functional theory. Phys Rev Lett 95:203004
71. Gross EKU, Dobson JF, Petersilka M (1996) Density functional theory of time-dependent phenomena. In: Nalewajski RF (ed) Density functional theory (Topics in Current Chemistry, vol 181). Springer, Berlin
72. Casida ME (1995) Time-dependent density functional response theory for molecules. In: Chong DP (ed) Recent advances in density functional methods, part I. World Scientific, Singapore
73. Mundt M, Kümmel S (2007) Photoelectron spectra of anionic sodium clusters from time-dependent density-functional theory in real time. Phys Rev B 76:035413
74. Castro A, Marques MAL, Rubio A (2004) Propagators for the time-dependent Kohn-Sham equations. J Chem Phys 121:3425
75. Ehrler OT, Weber JM, Furche F, Kappes MM (2003) Photoelectron spectroscopy of C_{84} dianions. Phys Rev Lett 91:113006
76. Moseler M, Huber B, Häkkinen H, Landman U, Wrigge G, Hoffmann MA, von Issendorff B (2003) Thermal effects in the photoelectron spectra of NaN^- clusters ($N = 419$). Phys Rev B 68:165413

77. Issendorff BV (2007) Phys Rev B 76:035413
78. Duffy P, Chong DP, Casida ME, Salahub DR (1994) Assessment of Kohn–Sham density-functional orbitals as approximate Dyson orbitals for the calculation of electron-momentum-spectroscopy scattering cross sections. Phys Rev A 50:4707
79. Baerends EJ, Gritsenko OV (1997) A quantum chemical view of density functional theory. J Phys Chem A 101:5383
80. Baerends EJ (2000) Perspective on 'self-consistent equations including exchange and correlation effects'. Theor Chem Acc 103:1265
81. Stowasser R, Hoffmann R (1999) What do the kohn-sham orbitals and eigenvalues mean? J Am Chem Soc 121:3414
82. Humeniuk A, Wohlgemuth M, Suzuki T, Mitrić R (2013) Time-resolved photoelectron imaging spectra from non-adiabatic molecular dynamics simulations. J Chem Phys 82:134104
83. Ullrich CA, Reinhard P-G, Suraud E (1997) Metallic clusters in strong femtosecond laser pulses. J Phys B At Mol Opt Phys 30:5043
84. Telnov DA, Chu S (2009) Effects of multiple electronic shells on strong-field multiphoton ionization and high-order harmonic generation of diatomic molecules with arbitrary orientation: an all-electron time-dependent density-functional approach. Phys Rev A 80:043412
85. Thiele M, Gross EKU, Kümmel S (2008) Adiabatic approximation in nonperturbative time-dependent density-functional theory. Phys Rev Lett 100:153004
86. Pohl A, Reinhard P-G, Suraud E (2000) Towards single-particle spectroscopy of small metal clusters. Phys Rev Lett 84:5090
87. Vincendon M, Dinh PM, Romaniello P, Reinhard P-G, Suraud E (2013) Photoelectron spectra from full time dependent self-interaction correction. Eur Phys J D 67:97
88. Goldberg A, Shore BW (1978) Modelling laser ionisation. J Phys B Atom Mol Phys 11:3339
89. Reinhard P-G, Stevenson PD, Almehed D, Maruhn JA, Strayer MR (2006) Role of boundary conditions in dynamic studies of nuclear giant resonances and collisions. Phys Rev E 73:036709
90. De Giovannini U, Varsano D, Marques MAL, Appel H, Gross EKU, Rubio A (2012) Ab-initio angle and energy resolved photoelectron spectroscopy with time-dependent density-functional theory. Phys Rev A 85:062515
91. Dauth M, Kümmel S (2013) (submitted for publication)
92. Lein M, Gross EKU, Engel V (2000) Intense-field double ionization of helium: identifying the mechanism. Phys Rev Lett 85:4707
93. Levy M, Perdew JP, Sahni V (1984) Exact differential equation for the density and ionization energy of a many-particle system. Phys Rev A 30:2745
94. Almbladh CO, von-Barth U (1985) Exact results for the charge and spin densities, exchange-correlation potentials, and density-functional eigenvalues. Phys Rev B 31:3231
95. Perdew JP, Parr RG, Levy M, Balduz JL (1982) Density-functional theory for fractional particle number: derivative discontinuities of the energy. Phys Rev Lett 49:1691
96. Perdew JP, Levy M (1987) Comment on 'significance of the highest occupied Kohn-Sham eigenvalue'. Phys Rev B 56:16021
97. Koopmans TC (1934) Über die Zuordnung von Wellenfunktionen und Eigenwerten zu den Einzelnen Elektronen Eines Atoms. Physica 1:104
98. Sham LJ, Kohn W (1966) One-particle properties of an inhomogeneous interacting electron gas. Phys Rev 145:561
99. Sham LJ, Schlüter M (1983) Density-functional theory of the energy gap. Phys Rev Lett 51:1888
100. Casida ME (1995) Generalization of the optimized-effective-potential model to include electron correlation: a variational derivation of the Sham-Schlüter equation for the exact exchange-correlation potential. Phys Rev A 51:2005
101. Jones RO, Gunnarsson O (1989) The density functional formalism, its applications and prospects. Rev Mod Phys 61:68

102. Hedin L, Lundqvist S (1969) Effects of electron-electron and electron-phonon interactions on the one-electron states of solids. Solid State Phys 23:1
103. Chong DP, Gritsenko OV, Baerends EJ (2002) Interpretation of the Kohnsham orbital energies as approximate vertical ionization potentials. J Chem Phys 116:1760
104. Perdew JP, Levy M (1983) Physical content of the exact Kohn-Sham orbital energies: band gaps and derivative discontinuities. Phys Rev Lett 51:1884
105. Sagvolden E, Perdew JP (2008) Discontinuity of the exchange-correlation potential: support for assumptions used to find it. Phys Rev A 77:01251
106. Godby RW, Schluter M, Sham LJ (1986) Accurate exchange-correlation potential for silicon and its discontinuity on addition of an electron. Phys Rev Lett 56:2415
107. Godby RW, Schlüter M, Sham LJ (1987) Trends in self-energy operators and their corresponding exchange-correlation potentials. Phys Rev B 36:6497
108. Chan GKL (1999) A fresh look at ensembles: derivative discontinuities in density functional theory. J Chem Phys 110:4710
109. Allen MJ, Tozer D (2002) Eigenvalues, integer discontinuities and NMR shielding constants in Kohn-Sham theory. J Mol Phys 100:433
110. Teale AM, De Proft F, Tozer DJ (2008) Orbital energies and negative electron affinities from density functional theory: insight from the integer discontinuity. J Chem Phys 129:044110
111. Kümmel S, Kronik L (2008) Orbital-dependent density functionals: theory and applications. Rev Mod Phys 80:3
112. Kronik L, Stein T, Refaely-Abramson S, Baer R (2012) Excitation gaps of finite-sized systems from optimally tuned range-separated hybrid functionals. J Chem Theory Comput 8:1515
113. Hellgren M, Gross EKU (2012) Discontinuities of the exchange-correlation kernel and charge-transfer excitations in time-dependent density-functional theory. Phys Rev A 85:022514
114. Perdew JP (1986) Density functional theory and the band gap problem. Int J Quant Chem 19:497
115. Perdew JP, Kurth S (2003) Density functionals for non-relativistic coulomb systems in the new century. In: Fiolhais C, Nogueira F, Marques MAL (eds) A primer in density functional theory. Springer, Berlin
116. Perdew JP, Burke K, Ernzerhof M (1996) Generalized gradient approximation made simple. Phys Rev Lett 77:3865
117. Becke AD (1988) Density-functional exchange-energy approximation with correct asymptotic behavior. Phys Rev A 38:3098
118. Lee C, Yang W, Parr RG (1988) Development of the Colle-Salvetti correlation-energy formula into a functional of the electron density. Phys Rev B 37:785
119. Borgoo A, Teale AM, Tozer DJ (2012) Effective homogeneity of the exchange-correlation and non-interacting kinetic energy functionals under density scaling. J Chem Phys 136:034101
120. Tozer DJ (1998) Effective homogeneity of the exchange-correlation energy functional. Phys Rev A 58:3524
121. Kraisler E, Kronik L (2013) Piecewise linearity of approximate density functionals revisited: implications for frontier orbital energies. Phys Rev Lett 110:126403
122. Cohen AJ, Mori-Sánchez P, Yang W (2008) Insights into current limitations of density functional theory. Science 321:792
123. Armiento R, Kümmel S (2013) Orbital localization, charge transfer, and band gaps in semilocal density-functional theory. Phys Rev Lett 111:036402
124. Apelbaum JA, Hamann DR (1973) Self-consistent pseudopotential for Si. Phys Rev B 8:1777
125. Glötzel D, Segall B, Andersen OK (1980) Self-consistent electronic structure of Si, Ge and diamond by the LMTO-ASA method. Solid State Comm 36:403
126. Kronik L, Fromherz R, Ko E, Ganteför G, Chelikowsky JR (2002) Electron affinity as a predictor of cluster anion structures. Nat Mater 1:49

127. Guliamov O, Kronik L, Jackson KA (2005) Photoelectron spectroscopy as a structural probe of intermediate size clusters. J Chem Phys 123:204312
128. Kronik L, Fromherz R, Ko E, Ganteför G, Chelikowsky JR (2003) Photoemission spectra of deuterated silicon clusters: experiment and theory. Eur Phys J D 24:33
129. Binggeli N, Martins JL, Chelikowsky JR (1992) Simulation of Si clusters via Langevin molecular dynamics with quantum forces. Phys Rev Lett 68:2956
130. Barnett RN, Landman U (1993) Born-Oppenheimer molecular-dynamics simulations of finite systems: structure and dynamics of H_2O_2. Phys Rev B 48:2081
131. Kümmel S, Akola J, Manninen M (2000) Thermal expansion in small metal clusters and its impact on the electric polarizability. Phys Rev Lett 84:3827
132. Kronik L, Vasiliev I, Chelikowsky JR (2000) Ab initio calculations for structure and temperature effects on the polarizabilities of Na_n ($n \leq 20$) clusters. Phys Rev B 62:9992
133. Marom N, Kim N, Chelikowsky JR (2012) Structure selection based on high vertical electron affinity for TiO_2 clusters. Phys Rev Lett 108:106801
134. Boschi R, Murrell JN, Schmidt W (1972) Photoelectron spectra of polycyclic aromatic hydrocarbons. Faraday Discuss Chem Soc 54:116
135. Körzdörfer T, Kümmel S (2010) Single-particle and quasiparticle interpretation of Kohn-Sham and generalized Kohn-Sham eigenvalues for hybrid functionals. Phys Rev B 82:155206
136. Refaely-Abramson S, Sharifzadeh S, Govind N, Autschbach J, Neaton JB, Baer R, Kronik L (2012) Quasiparticle spectra from a nonempirical optimally tuned range-separated hybrid density functional. Phys Rev Lett 109:226405
137. Körzdörfer T, Kümmel S, Marom N, Kronik L (2009) When to trust photoelectron spectra from Kohn-Sham eigenvalues: the case of organic semiconductors. Phys Rev B 79:201205 (R). (2010). Erratum: Phys Rev B 82:129903(E)
138. Ueno N, Koch N, Wee ATS (eds) (2013) The molecule-metal interface. Wiley-VCH, Weinheim
139. Segev L, Salomon A, Natan A, Cahen D, Kronik L, Amy F, Chan CK, Kahn A (2006) Electronic structure of Si(111)-bound alkyl monolayers: theory and experiment. Phys Rev B 74:165323
140. Hwang J, Kim EG, Liu J, Brédas JL, Duggal A, Kahn A (2007) Photoelectron spectroscopic study of the electronic band structure of polyfluorene and fluorene-arylamine copolymers at interfaces. J Phys Chem C 111:1378
141. Rinke P, Scheffler M, Qteish A, Winkelnkemper M, Bimberg D, Neugebauer J (2006) Band gap and band parameters of InN and GaN from quasiparticle energy calculations based on exact-exchange density-functional theory. Appl Phys Lett 89:161919
142. Fuchs F, Bechstedt F (2008) Indium-oxide polymorphs from first principles: quasiparticle electronic states. Phys Rev B 77:155107
143. Fermi E, Amaldi E (1934) Le Orbite oos degli elementi. Atti R Accad Naz Lincei Mem C1 Sci Fis. Mat Nat 6:119
144. Fermi E (1927) Un metodo statistico per la determinazione di alcune prioprieta dell'atomo. Rend Accad Naz Lincei 6:602
145. Thomas LH (1927) The calculation of atomic fields. Proc Camb Philos Soc 23:542
146. Nemykin VN, Hadt RG, Belosludov RV, Mizuseki H, Kawazoe Y (2007) Influence of molecular geometry, exchange-correlation functional, and solvent effects in the modeling of vertical excitation energies in phthalocyanines using time-dependent density functional theory (TDDFT) and polarized continuum model TDDFT methods: can modern computational chemistry methods explain experimental controversies? J Phys Chem 111:12901
147. Marom N, Hod O, Scuseria GE, Kronik L (2008) Electronic structure of copper phthalocyanine: a comparative density functional theory study. J Chem Phys 128:164107
148. Marom N, Kronik L (2009) Density functional theory of transition metal phthalocyanines. I: Electronic structure of NiPc and CoPc - self-interaction effects. Appl Phys A 95:159

149. Rissner F, Egger DA, Natan A, Körzdörfer KS, Kronik L, Zojer E (2011) Collectively induced quantum-confined stark effect in monolayers of molecules consisting of polar repeating units. J Am Chem Soc 133:18634
150. Körzdörfer T, Kümmel S, Mundt M (2008) Self-interaction correction and the optimized effective potential. J Chem Phys 129:014110
151. Hofmann D, Kümmel S (2012) Self-interaction correction in a real-time Kohn-Sham scheme: access to difficult excitations in time-dependent density functional theory. J Chem Phys 137:064117
152. Hofmann D, Klüpfel S, Klüpfel P, Kümmel S (2012) Using complex degrees of freedom in the Kohn-Sham self-interaction correction. Phys Rev A 85:062514
153. Pederson MR, Heaton RA, Lin CC (1984) Local-density Hartree-Fock theory of electronic states of molecules with self-interaction correction. J Chem Phys 80:1972
154. Pederson MR, Heaton RA, Lin CC (1985) Density-functional theory with self-interaction correction: application to the lithium molecule. J Chem Phys 82:2688
155. Pederson MR, Heaton RA, Lin CC (1988) Localized and canonical atomic orbitals in self-interaction corrected local density functional approximation. J Chem Phys 88:1807
156. Vydrov OA, Scuseria GE, Perdew JP (2007) Tests of functionals for systems with fractional electron number. J Chem Phys 126:154109
157. Sharp RT, Horton GK (1953) A variational approach to the unipotential many-electron problem. Phys Rev 90:317
158. Talman JD, Shadwick WF (1976) Optimized effective atomic central potential. Phys Rev A 14:36
159. Sahni V, Gruenebaum J, Perdew JP (1982) Study of the density-gradient expansion for the exchange energy. Phys Rev B 26:4731
160. Grabo T, Kreibich T, Gross EKU (1997) Optimized effective potential for atoms and molecules. Mol Eng 7:27
161. Körzdörfer T, Mundt M, Kümmel S (2008) Electrical response of molecular systems: the power of self-interaction corrected Kohn-Sham theory. Phys Rev Lett 100:133004
162. Puschnig P, Berkebile S, Fleming AJ, Koller G, Emtsev K, Seyller T, Riley JD, Ambrosch-Draxl C, Netzer FP, Ramsey MG (2009) Reconstruction of molecular orbital densities from photoemission data. Science 326:702
163. Dauth M, Körzdörfer T, Kümmel S, Ziroff J, Wiessner M, Schöll A, Reinert F, Arita M, Shimada K (2011) Orbital density reconstruction for molecules. Phys Rev Lett 107:193002
164. Becke AD (1993) A new mixing of Hartree-Fock and local density-functional theories. J Chem Phys 98:1372
165. Becke AD (1993) Density-functional thermochemistry. III. The role of exact exchange. J Chem Phys 98:5648
166. Perdew JP, Ernzerhof M, Burke K (1996) Rationale for mixing exact exchange with density functional approximations. J Chem Phys 105:9982
167. Adamo C, Barone V (1999) Toward reliable density functional methods without adjustable parameters: The PBE0 model. J Chem Phys 110:6158
168. Ernzerhof M, Scuseria GE (1999) Assessment of the Perdew-Burke-Ernzerhof exchange-correlation functional. J Chem Phys 110:5029
169. Stephens PJ, Devlin FJ, Chabalowski FC, Frisch MJ (1994) Ab initio calculation of vibrational absorption and circular dichroism spectra using density functional force fields. J Phys Chem 98:11623
170. Corá F, Alfredsson M, Mallia G, Middlemiss DS, Mackrodt WC, Dovesi R, Orlando R (2004) The performance of hybrid density functionals in solid state chemistry. Struct Bond 113:171
171. Paier J, Marsman M, Hummer K, Kresse G, Gerber IC, Ángyán JG (2006) Screened hybrid density functionals applied to solids. J Chem Phys 124:154709
172. Staroverov VN, Scuseria GE, Tao J, Perdew JP (2003) Comparative assessment of a new nonempirical density functional: molecules and hydrogen-bonded complexes. J Chem Phys 119:12129

173. Seidl A, Görling A, Vogl P, Majewski JA, Levy M (1996) Generalized Kohn–Sham schemes and the band-gap problem. Phys Rev B 53:3764
174. Görling A, Levy M (1997) Hybrid schemes combining the Hartree-Fock method and density-functional theory: underlying formalism and properties of correlation functionals. J Chem Phys 107:2675
175. Baer R, Livshits E, Salzner U (2010) Tuned range-separated hybrids in density functional theory. Annu Rev Phys Chem 61:85
176. Stein T, Autschbach J, Govind N, Kronik L, Baer R (2012) Curvature and frontier orbital energies in density functional theory. J Phys Chem Lett 3:3740
177. Grüning M, Marini A, Rubio A (2006) Effect of spatial nonlocality on the density functional band gap. Phys Rev B 74:161103
178. Blase X, Attaccalite C, Olevano V (2011) First-principles GW calculations for fullerenes, porphyrins, phtalocyanine, and other molecules of interest for organic photovoltaic applications. Phys Rev B 83:115103
179. Refaely-Abramson S, Baer R, Kronik L (2011) Fundamental and excitation gaps in molecules of relevance for organic photovoltaics from an optimally tuned range-separated hybrid functional. Phys Rev B 84:075144
180. Marom N, Tkatchenko A, Scheffler M, Kronik L (2010) Describing both dispersion interactions and electronic structure using density functional theory: the case of metal-phthalocyanine dimers. J Chem Theory Comput 6:81
181. Yasuhara H, Takada Y (1991) Analysis of the self-energy for an electron gas and a proposal of an improved exchange and correlation potential for band calculations. Phys Rev B 43:7200
182. van Schilfgaarde M, Sher A, Chen AB (1997) Theory of A1N, GaN, InN and their alloys. J Cryst Growth 178:8
183. Palummo M, Hogan C, Sottile F, Bagala P, Rubio AJ (2009) Ab initio electronic and optical spectra of free-base porphyrins: the role of electronic correlation. J Chem Phys 131:084102
184. Stradi D, Díaz C, Martn F, Alcamí M (2011) A density functional theory study of the manganese-phthalocyanine. Theor Chem Acc 128:497
185. Brena B, Puglia C, de Simone M, Coreno M, Tarafder K, Feyer V, Banerjee R, Göthelid E, Sanyal B, Oppeneer PM, Eriksson O (2011) Valence-band electronic structure of iron phthalocyanine: an experimental and theoretical photoelectron spectroscopy study. J Chem Phys 134:074312
186. Marom N, Ren X, Moussa JE, Chelikowsky JR, Kronik L (2011) Electronic structure of copper phthalocyanine from G_0W_0 calculations. Phys Rev B 84:195143
187. Salomon E, Amsalem P, Marom N, Vondracek M, Kronik L, Koch N, Angot T (2013) Electronic structure of CoPc adsorbed on Ag(100): evidence for molecule-substrate interaction mediated by Co 3d orbitals. Phys Rev B 87:075407
188. Toher C, Filippetti A, Sanvito S, Burke K (2005) Self-interaction errors in density-functional calculations of electronic transport. Phys Rev Lett 95:146402
189. Cehovin A, Mera H, Jensen JH, Stokbro K, Pedersen TB (2008) Role of the virtual orbitals and HOMO-LUMO gap in mean-field approximations to the conductance of molecular junctions. Phys Rev B 77:195432
190. Quek SY, Choi HJ, Louie SG, Neaton JB (2009) Length dependence of conductance in aromatic single-molecule junctions. Nano Lett 9:3949
191. Strinati G (1988) Application of the Greens functions method to the study of the optical properties of semiconductors. Riv Nuovo Cimento 11:1
192. Tozer DJ (2003) Relationship between long-range charge-transfer excitation energy error and integer discontinuity in Kohn-Sham theory. J Chem Phys 119:12697
193. Stein T, Kronik L, Baer R (2009) Reliable prediction of charge transfer excitations in molecular complexes using time-dependent density functional theory. J Am Chem Soc 131:2818
194. Stein T, Kronik L, Baer R (2009) Prediction of charge-transfer excitations in coumarin-based dyes using a range-separated functional tuned from first principles. J Chem Phys 131:244119

195. Karolewski A, Stein T, Baer R, Kümmel S (2011) Tailoring the optical gap in light-harvesting molecules. J Chem Phys 134:151101
196. Risko C, Brédas JL (2013) Small optical gap molecules and polymers: using theory to design more efficient materials for organic photovoltaics. Top Curr Chem. doi:10.1007.128.2013.459, in press
197. Stein T, Eisenberg H, Kronik L, Baer R (2010) Fundamental gaps in finite systems from eigenvalues of a generalized Kohn-Sham method. Phys Rev Lett 105:266802
198. Leininger T, Stoll H, Werner HJ, Savin A (1997) Combining long-range configuration interaction with short-range density functionals. Chem Phys Lett 275:151
199. Savin A (1995) Beyond the Kohn-Sham determinant. In: Chong DP (ed) Recent advances in density functional methods, part I. World Scientific, Singapore
200. Savin A, Flad HJ (1995) Density functionals for the Yukawa electron-electron interaction. Int J Quantum Chem 56:327
201. Iikura H, Tsuneda T, Yanai T, Hirao K (2001) A long-range correction scheme for generalized-gradient-approximation exchange functionals. J Chem Phys 115:3540
202. Yanai T, Tew DP, Handy NC (2004) A new hybrid exchange-correlation functional using the coulomb-attenuating method (CAM-B3LYP). Chem Phys Lett 393:51
203. Vydrov OA, Scuseria GE (2006) Assessment of a long-range corrected hybrid functional. J Chem Phys 125:234109
204. Cohen AJ, Mori-Sanchez P, Yang WT (2007) Development of exchange-correlation functionals with minimal many-electron self-interaction error. J Chem Phys 126:191109
205. Chai JD, Head-Gordon M (2008) Systematic optimization of long-range corrected hybrid density functionals. J Chem Phys 128:084106
206. Chai JD, Head-Gordon M (2008) Long-range corrected hybrid density functionals with damped atom–atom dispersion corrections. Phys Chem Chem Phys 10:6615
207. Rohrdanz MA, Martins KM, Herbert JM (2009) A long-range-corrected density functional that performs well for both ground-state properties and time-dependent density functional theory excitation energies, including charge-transfer excited states. J Chem Phys 130:054112
208. Baer R, Neuhauser D (2005) Density functional theory with correct long-range asymptotic behavior. Phys Rev Lett 94:043002
209. Livshits E, Baer R (2007) A well-tempered density functional theory of electrons in molecules. Phys Chem Chem Phys 9:2932
210. Salzner U, Baer R (2009) Koopmans springs to life. J Chem Phys 131:231101
211. Karolewski A, Kronik L, Kümmel S (2013) Using optimally tuned range separated hybrid functionals in ground-state calculations: consequences and caveats. J Chem Phys 138:204115
212. Sini G, Sears JS, Brédas JL (2011) Evaluating the performance of DFT functionals in assessing the interaction energy and ground-state charge transfer of donor/acceptor complexes: tetrathiafulvalene-tetracyanoquinodimethane (TTF-TCNQ) as a model case. J Chem Theory Comput 7:602
213. Körzdörfer T, Sears JS, Sutton C, Brédas JL (2011) Long-range corrected hybrid functionals for π-conjugated systems: dependence of the range-separation parameter on conjugation length. J Chem Phys 135:204107
214. Phillips H, Zheng S, Hyla A, Laine R, Goodson T, Geva E, Dunietz BD (2012) Ab initio calculation of the electronic absorption of functionalized octahedral silsesquioxanes via time-dependent density functional theory with range-separated hybrid functionals. J Phys Chem A 116:1137
215. Foster ME, Wong BM (2012) Nonempirically tuned range-separated DFT accurately predicts both fundamental and excitation gaps in DNA and RNA nucleobases. J Chem Theory Comput 8:2682
216. Srebro M, Autschbach J (2012) Does a molecule-specific density functional give an accurate electron density? The challenging case of the CuCl electric field gradient. J Phys Chem Lett 3:576

217. Moore B, Autschbach J (2012) Density functional study of tetraphenylporphyrin long-range exciton coupling. Chem Open 1:184
218. Moore B, Srebro M, Autschbach J (2012) Analysis of optical activity in terms of bonds and lone-pairs: the exceptionally large optical rotation of norbornenone. J Chem Theory Comput 8:4336
219. Sun H, Autschbach J (2013) Influence of the delocalization error and applicability of optimal functional tuning in density functional calculations of nonlinear optical properties of organic donoracceptor chromophores. Chem Phys Chem 14:2450
220. Gledhill JD, Peach MGJ, Tozer DJ (2013) Assessment of tuning methods for enforcing approximate energy linearity in range-separated hybrid functionals. J Chem Theory Comput 9:4414
221. Cococcioni M, de Gironcoli S (2005) Linear response approach to the calculation of the effective interaction parameters in the LDA+U method. Phys Rev B 71:035105
222. Lany S, Zunger A (2009) Polaronic hole localization and multiple hole binding of acceptors in oxide wide-gap semiconductors. Phys Rev B 80:085202
223. Dabo I, Ferretti A, Poilvert N, Li YL, Marzari N, Cococcioni M (2010) Koopmans' condition for density-functional theory. Phys Rev B 82:115121
224. Dabo I, Ferretti A, Park CH, Poilvert N, Li YL, Cococcioni M, Marzari N (2013) Donor and acceptor levels of organic photovoltaic compounds from first principles. Phys Chem Chem Phys 15:685
225. Flores F, Abad E, Martínez JI, Pieczyrak B, Ortega J (2013) On the organic energy gap problem. J Phys Condens Matter 25:094007
226. Zheng X, Zhou T, Yang W (2013) A nonempirical scaling correction approach for density functional methods involving substantial amount of Hartree–Fock exchange. J Chem Phys 138:174105
227. Heyd J, Scuseria GE, Ernzerhof M (2003) Hybrid functionals based on a screened Coulomb potential. J Chem Phys 118:8207
228. Krukau A, Vydrov O, Izmaylov A, Scuseria GE (2006) Influence of the exchange screening parameter on the performance of screened hybrid functionals. J Chem Phys 125:224106
229. Janesko BG, Henderson TM, Scuseria GE (2009) Screened hybrid density functionals for solid-state chemistry and physics. Phys Chem Chem Phys 11:443
230. Ren J, Meng S, Wang YL, Ma XC, Xue QK, Kaxiras E (2011) Properties of copper (fluoro-) phthalocyanine layers deposited on epitaxial graphene. Chem Phys 134:194706
231. Bisti F, Stroppa A, Picozzi S, Ottaviano S (2011) Fingerprints of the hydrogen bond in the photoemission spectra of croconic acid condensed phase: an X-ray photoelectron spectroscopy and ab-initio study. J Chem Phys 134:174505
232. Bisti F, Stroppa A, Donarelli M, Picozzi S, Ottaviano S (2011) Electronic structure of tris (8-hydroxyquinolinato)aluminium(III) revisited using the Heyd-Scuseria-Ernzerhof hybrid functional: theory and experiments. Phys Rev B 84:195112
233. Bisti F, Stroppa A, Perrozzi F, Donarelli M, Picozzi S, Coreno M, de Simone M, Prince KC, Ottaviano S (2013) The electronic structure of gas phase croconic acid compared to the condensed phase: more insight into the hydrogen bond interaction. J Chem Phys 138:014308
234. Lucero MJ, Henderson TM, Scuseria GE (2012) Improved semiconductor lattice parameters and band gaps from a middle-range screened hybrid exchange functional. J Phys Condens Matter 24:145504
235. Körzdörfer T, Parrish RM, Marom N, Sears JS, Sherrill CD, Brédas JL (2012) Assessment of the performance of tuned range-separated hybrid density functionals in predicting accurate quasiparticle spectra. Phys Rev B 86:205110
236. Egger DA, Weissman S, Refaely-Abramson S, Sharifzadeh S, Dauth M, Baer R, Kümmel S, Neaton JB, Zojer E, Kronik L (2014) Outer-valence electron spectra of prototypical aromatic heterocycles from an optimally-tuned range-separated hybrid functional. J Chem Theo Comp, in press. http://dx.doi.org/10.1021/ct400956h
237. Salzner U, Aydin A (2011) Improved prediction of properties of π-conjugated oligomers with range-separated hybrid density functionals. J Chem Theory Comput 7:2568